LBL-12849

Lawrence Berkeley Laboratory
UNIVERSITY OF CALIFORNIA

Materials & Molecular Research Division

PRE EUTECTIC DENSIFICATION IN MgF_2 - CaF_2

Sing-Chung Hu
(M.S. thesis)

May 1981

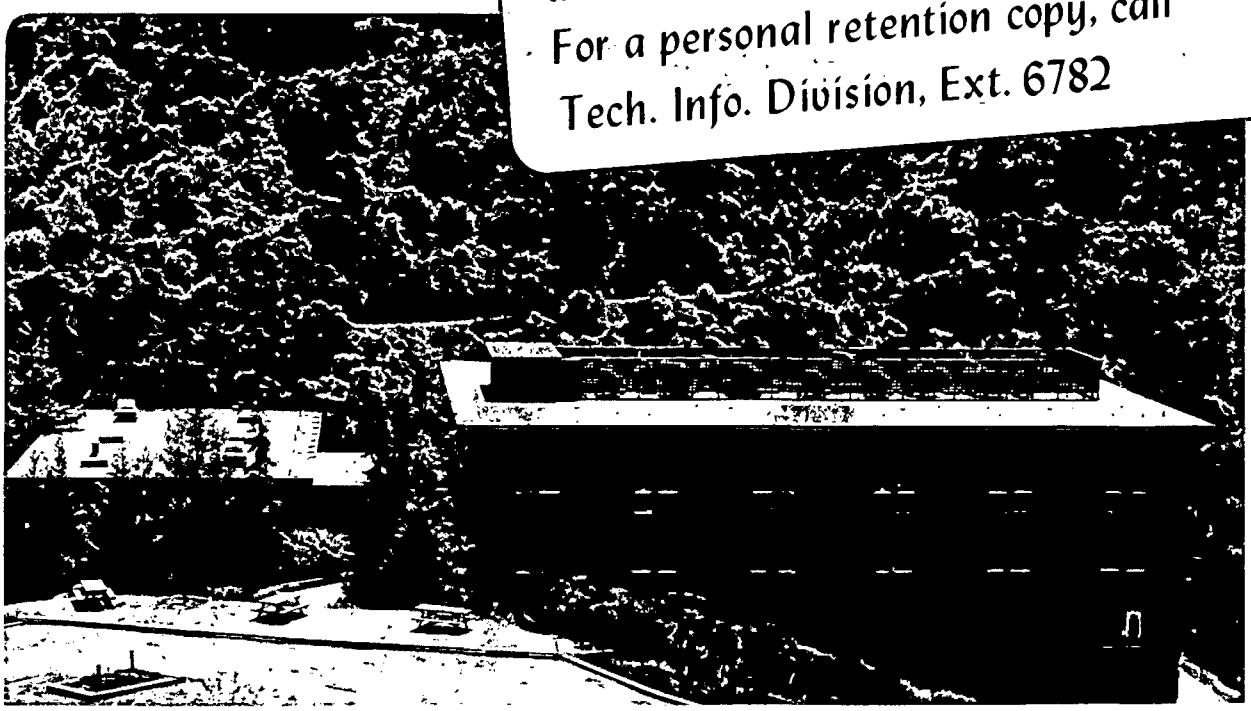

Prepared for the U.S. Department of Energy under Contract W-7405-ENG-48

DISCLAIMER

LBL-12849

PRE EUTECTIC DENSIFICATION IN MgF_2 - CaF_2

Sing-Chung Hu

Materials and Molecular Research Division,
Lawrence Berkeley Laboratory and
Department of Materials Science and Mineral Engineering,
University of California,
Berkeley, California 94720

May, 1981

This work was supported by the Director, Office of Energy Research, Office of Basic Energy Sciences, Materials Sciences Division of the U.S. Department of Energy under Contract No. W-7405-ENG-48.

PRE EUTECTIC DENSIFICATION IN MgF_2 - CaF_2

Contents

Pre Eutectic Densification in MgF_2 - CaF_2

Sing-Chung Hu

Materials and Molecular Research Division,
Lawrence Berkeley Laboratory and
Department of Materials Science and
Mineral Engineering, University of California,
Berkeley, California.

ABSTRACT

Although most people attributed the effect of a eutectic additive on the sintering process to liquid phase sintering, pre-eutectic densification phenomena may also be observed. In this work, the MgF_2 - CaF_2 system was chosen because of its simple phase diagram and low eutectic temperature ($\simeq$ 980°C).

Three sintering methods were used : (a) Arrested zone sintering, (b) constant heating rate sintering and (c) constant temperature sintering. Microstructural evolution and shrinkage vs temperature behaviour were studied.

It was found that the sintering rate of MgF_2 was enhanced by CaF_2 eutectic additive, and that the enhancement of sintering started at about 200°C below the eutectic temperature. The effectness of CaF_2 saturates at about 1 wt.%. By comparing the diffusivities obtained from diffusion experiment and constant temperature sintering experiment, it is concluded that the enhanced pre-eutectic densification kinetics result from increased solid state grain boundary transport due to eutectic forming phase.

The possible effect of oxidation on the eutectic temperature of CaF_2 - MgF_2 during the experiment, has been verified to strengthen the conclusion that solid state mass transport causes the enhancement. Auger analysis shows that Ca^{+2} is enriched at grain boundaries in a layer with a thickness of about 100 Å.

I. INTRODUCTION :

Although sintering of ceramic materials has been carried out for a long time, and the theory of sintering has also been studied extensively, the recent attempts at exploiting special properties of refractory materials (such as high energy density storage batteries, turbine blades, laser windows etc.) have necessitated a more profound understanding of the fundamental principles of ceramic fabrication. From an energy conservation point of view, more effective sintering processes should be developed to lower both sintering temperature and shorten sintering time. One promising method is liquid phase or transient liquid phase sintering. During such a sintering process, a modest amount of liquid phases form, and accelerate the densification of the ceramic. In past work on eutectic additive sintering of beta-alumina solid electrolytes[1,2,3] for use in the sodium/sulphur battery, a higher densification rate was observed, as is shown in Fig. 1. This led to the postulate that transient liquid phases might be active during the densification of sodium beta-alumina [4]. However, further experiments showed that anomalously rapid densification rates also occured below the temperature at which the eutectic phase was supposed to be melting. Such phenomena and the fact that only a very small amount of eutectic additive is necessary to achieve drastic densification rate increases, cannot be understood in the framework of the

liquid phase sintering theories. For example, Kingery's liquid phase sintering model [5] suggested that a continuous thin liquid film formed between solid particles to provide a fast mass transport path thereby greatly increasing the sintering rate. Unless the liquid completly pentrates between each of the solid particles, directly joining at the particle contact points will occur. Then, for particle centers to move closer together (as is required for shrinkage), sintering must occur by the transfer of material within the solid phase. In liquid phase sintering, material transfer may take place by a solution-repreciptation process in which material is dissolved away from contact points and is transfered through the liquid, thus allowing the centers of particles to approach each other. Lenel[6], Gurland and Norton[7], and Cannon and Lenel[8] agree that : (a) an appreciable amount of liquid; (b) an appreciable solubility of the solid in liquid; and (c) complete wetting are requirements for enhancing densification kinectics. However, all these liquid phase mechanisms can not explain the densification rate increase below eutectic temperature in which the liquid is not yet formed.

In Gessinger et al's work [9] on sintering of tungsten with nickel additions, it was suggested that the activating effect of nickel on the sintering of 0.5 μm tungsten powder at 1000°C is due to the enhancement of grain boundary self-diffusion in tungsten. Brophy et. al. [10] have proposed a detailed theory of the various stages leading to

densification of tungsten-nickel compacts. In the first stage, nickel (which has a low solubility in tungsten) appears to serve as a carrier phase through which tungsten atoms can move rapidly. From measurements of the amount of nickel required to attain "full activation" of sintering, which means that the effect of activation is saturated when the additive amount exceeds some limit value, he concluded that a monoatomic layer of nickel, evenly distributed over the entire surface of the tungsten particles, acts as the carrier phase (Fig. 2). Basically, the suggested mechanism of densification resembles that of liquid phase sintering [5] with the solid nickel film playing the role of a completely wetting phase. Schintlmeister and Richter [11] studied the grain boundary diffusion of radioactive tungsten in pure and nickel-doped tungsten compacts, and found that the presence of nickel in the grain boundaries increased the grain boundary diffusion rate. In Exner's work [12] on sintering of WC-Co mixture, it was found that the WC-Co mixtures continued shrinkage up to more than 95% relative density in the solid state while only a few additional percent of densification were achieved above the melting point.

From the above, it is believed that, below the eutectic temperature of two phase powders, there may be some abnormally rapid solid state mass transport either (a) in the grain boundaries between joining particle in contact with an eutectic forming phase; or (b) through the bulk of the "alloy" particles into which the eutectic forming component

had diffused . In other words, only grain boundary diffusion and volume diffusion mechanisms can account for the rapid densification phenomena below the eutectic temperature in a two components powder compact. The aim of this work was to find which mechanism dominated when an eutectic forming component was added to a powder. The MgF_2 - CaF_2 system was selected because of its simple phase diagram [13] (Fig. 3.) and low eutectic temperature ($\simeq$ 980 ^{o}C).

In order to clarify which mechanism dominated the densification rate below the eutectic temperature , three methods were used: (a) arrested zone sintering (AZS) to get a continuous microstructural evolution as function of sintering history, (b) constant heating rate sintering (CHR) to obtain a more accurate sintering rate vs temperature at different heating rates for various amounts of eutectic additive, and (c) constant temperature sintering (CTS) to provide the diffusion data allowing an analysis of the possible sintering mechanism and its apparent activation energy.

Kingery and Berg [14], Coble [15], and Johnson and Clarke [16] theoretically determined the relation between shrinkage and time at a given temperature for different possible mechanisms by considering simple geometric models. Coble [15] offered the sintering equation in general form as follows :

$$\left(\frac{\Delta L}{L_o}\right)^p = \left(\frac{BD\gamma\delta^3}{r^m kT}\right)t \qquad \langle 1 \rangle$$

where $\Delta L/L_o$ = fractional shrinkage under isothermal condition; p = time independent exponent; B = rate constants which can be calculated for the different geometries; D = diffusion coefficient; γ = surface energy; δ^3 = vacancy volume; r = particle size; m = size-effect constants; k = Boltzmann's constant; T = absolute temperature; t = time. If we take

$$K_o = \frac{BD\gamma\delta^3}{r^m kT} \quad ; \quad n = \frac{1}{p} \quad ; \quad \text{and } k_o = K_o^n$$

then Eq. <1> can be written as

$$\frac{\Delta L}{L_o} = k_o t^n \qquad \langle 2 \rangle$$

where k_o is a constant depending on temperature, particle size and characteristics of the materials; n=1/p is the time exponent. So Eq. <2> is exactly the same as Eq. <1>. Experimental data generally follow the form of Eq. <2> [17]. Hence it would be possible to compare experimentally determined values of the exponent n with those predicted by different theories. If there is agreement between the empirically determined exponent and one calculated theoretically, one can reasonably assume that the effective mechanism responsible for sintering is that given by the model in agreement with experiment.

From

$$k_o = K_o^n = \left(\frac{BD\gamma\delta^3}{r^m kT}\right)^n$$

$$= \left(\frac{B\gamma\delta^3}{r^m k}\right)^n \left(\frac{D^n}{T^n}\right)$$

Let

$$k' = \left(\frac{B\gamma\delta^3}{r^m k}\right)^n$$

$$k_o = \frac{k'}{T^n} D^n \qquad \langle 3 \rangle$$

where k' is a constant independent of temperature.

Thus if sintering is governed by diffusion then the paramenter k_o can be represented by a theoretical expression of the form shown in Eq. <3>. Taking the natural log of both sides of Eq. <3> and writing

$$D = D_o \exp\left(-\frac{Q}{RT}\right)$$

we have

$$\ln k_o = \ln(k' D_o^n) - n\ln T - \left(\frac{nQ}{RT}\right) \qquad \langle 4 \rangle$$

Let $k' D_o^n = k''$ and

$$\ln k_q = \ln k_o + n\ln T$$

Eq. <4> becomes

$$\ln k_q = \ln k'' - \frac{nQ}{RT} \qquad <5>$$

The final form would be

$$k_q = k'' \exp(-\frac{nQ}{RT}) \qquad <6>$$

where Q is the activation energy for diffusion, and R is the gas constant. A plot of 1/n log k_q as a function of 1/T allows verification that shrinkage is a thermally activated process for which the activation energy is given by the slope of the curve. This activation energy can then be compared to the one determined or expected for grain boundary or bulk mass transport.

Although the above method seems to be plausible, Johnson [18], who developed that method, pointed out that surface diffusion may affect the slope n and activation energy Q. He concluded that the slope of the logarithm shrinkage / logarithm time plot is a completely unreliable indicator of the sintering mechanism. The slope on time corrected plots for a grain boundary transport mechanism can vary from 0.33 upward as a result of a combination of surface diffusion or volume diffusion with the grain boundary diffusion.

If we take

$$n = \frac{1}{p} \quad ; \quad y = \frac{\Delta L}{L_o}$$

Johnson and Clarke [16] wrote down the sintering equation as follow :

(a) For volume diffusion only, Eq. <1> becomes

$$y \simeq \left(\frac{5.34\gamma\delta^3 D_v}{kTr^3}\right)^{0.49} t^{0.49} \qquad \langle 7 \rangle$$

(b) For grain boundary diffusion only,

$$y \simeq \left(\frac{2.14\gamma\delta^3 bD_b}{kTr^4}\right)^{0.33} t^{0.33} \qquad \langle 8 \rangle$$

where D_v = volume diffusion coefficient; b = grain boundary width; D_b = grain boundary diffusion coefficient; γ, k, T, r, t have the same meaning as in Eq. <1>.

From CTS experiment, we can get y, T, t, r. By reasonalbe estimation of γ and δ^3, we can calculate D_v or bD_b from Eq. <7>, <8>.

Since there is no interdiffusion data for MgF_2 - CaF_2 available in the literature, a simple diffusion experiment was conducted and the diffusion coefficient was estimated from

$$x = (Dt)^{1/2} \qquad \langle 9 \rangle$$

where x = diffusion distance; D = diffusion coefficent at experiment temperature T; t = diffusion time. The diffusion coefficients in the CTS experiments were estimated from the diffusion experiment from

$$D = D_o \exp(-\frac{Q}{RT}) \qquad <10>$$

where Q = estimated activation energy for diffusion.

The diffusion coefficient derived from CTS experiments (from Eq. <7>,<8>), are then to be compared to those derived from the diffusion experiment. From this comparison, it should be possible to determine if either volume diffusion or grain boundary diffusion is dominating.

II. EXPERIMENTS :

A. Materials :

Magnesium fluoride from the Materials Research Corporation (Orangeburg, New York 10962) with a purity of 99.8% was selected. The chemical analysis from the Materials Research Corporation is shown in Table 1.. The agglomerate size was below 200 mesh (average agglomerate size is 3 μm). In a thermobalance experiment, some raw powder was heated at rate of 5°C/min., from room temperature to 300°C. A continuous weight loss was observed. The total weight loss of 10 wt.% was completed below 300°C. This weight loss could be attributed to water evaporation.

Calcium Floride form the Orion Chemical Co.(Hunt, Beach, CA 92646) with purity 99.999%, and agglomerate size 1.3 μm (Fig. 4a.), was chosen as the eutectic forming additive.

B. Processing :

The procedure for preparing specimens of MgF_2 and MgF_2 doped with CaF_2 have been shown in Fig. 5. First, the MgF_2 powder was classified with a Acucut air classifier. A fine powder with an agglomerate size of 2.5 μm, and a coarse

powder with aggolmerate size 10 μm was obtained (Fig. 4b,c).

Different amounts of CaF_2 were added to a MgF_2 powder slurry in ethyl alcohol , and the slurry was stir dryed and mixed at 80°C. EDAX (Energy Dispersive Analysis of X-ray) mapping showed uniform distribution of CaF_2. Both pure and mixed powders then were subjected to the same procedure, as follows : The powder was die pressed at 48,000 psi., to form a 1/2" diameter disc, with 0.15" height to a fixed green density of 55% theoretical. Then, these discs were calcined in a vacuum furnace at 350°C for 1 hour, at a total pressure of less than 10^{-3} torr. This drove off the water without oxidizing the florides. This is necessary since both CaF_2 and MgF_2 would react with water and oxygen during heating. The densification rates were measured with an LVDT (linear variable differential transducer), in a set-up designed to operate in vacuum (Fig. 6.).

The specimens were sintered by three different methods: (a) arrested zone sintering (AZS), (b) constant heating rate sintering (CHR) and (c) constant temperature sintering (CTS).

C. Arrested Zone Sintering (AZS) :

Arrested Zone Sintering was developed by De Jonghe and Goo [1]. The microstructural evolution and local shrinkage

was examined for long samples partially fed into the hot zone of the furnace kept at some fixed temperature.

In the present experiment, both pure MgF_2 and eutectic additive specimen were pressed into discs, then marked and cut in half. They were positioned in rows, side by side, then put in the system, and fed into a heated furnace with the maximum temperature set at 1100°C. The feeding rate was kept at 0.2"/min. to minimize thermal impedance. The temperature profile of the furnace and heating rate of the specimens are shown in Fig. 7 and 8. The specimen temperature was determined by its location in the temperature profile. After sintering, the quartz tube was quickly withdrawn and the specimens were quenched rapidly. For comparison, shrinkage data were also obtained by feeding only one short specimen into hot zone of furnace and recording the dimensional changes with a dilatometer (LVDT).

D. Verification of the Eutectic Temperature :

Two single crystals of MgF_2 and CaF_2 with two parallel surfaces were put together in the system with the LVDT attached, and put into the furnace. The furnace was heated up at a constant heating rate of 4.5°C/min. until an eutectic liquid formed. When the eutectic liquid formed there was a rapid dimensional change which could be detected readily by LVDT. The temperature was monitored at the same

time by a S-type thermocouple set close to the specimen.

Since the fluorides may be oxidized very easily, even in the vacuum sintering as in our experimental condition, some oxidation of CaF_2 and MgF_2 may occur. These oxides (MgO and CaO) may affect the eutectic temperature of CaF_2 - MgF_2 or may produce some other liquids below 980°C, so that the behaviour of a CaO-MgO-CaF_2-MgF_2 mix needed to be examined.

One simple experiment was conducted as follow : The eutectic composition of CaF_2 - MgF_2 (with 55.6 wt.% CaF_2) powder was prepared by stir-drying. 5 wt.% MgO and 5 wt.% CaO were added to above powder to form an oxide-eutectic mixture. The pure eutectic mixture and oxide-eutectic mixture powders were put into the vacuum furnace with thermocouple embeded into the powders, and were heated up to 1000°C at 4.5°C/min.. Both temperatures were recorded on a chart recorder. If there is liquid formed we should see some flat region on temperature vs time curve (temperature constant), as shown in Fig 15..

E. Constant Heating Rate Sintering (CHR) :

Specimens, after low temperature water removal, were put between two 1 mil. thick platinum discs to prevent reaction between the fluorides and quartz system. The linear heating rates were 4.5°C/min., 9°C/min. and 16°C/min.. The dimensional changes during heating were monitored by the

LVDT and the temperature was measured by a S-type thermocouple set close to specimen. Both the LVDT and thermocouple signals were recorded on a chart recorder (Fig. 6.). The microstructure of pure and eutectic additive containing specimen at different temperatures was obtained by heating the specimen at 4.5°C/min. to 800°C, 900°C or 1000°C and then quenching it by quickly withdrawing it from the furnace.

F. Constant Temperature Sintering (CTS) :

The specimens, after vacuum drying, were put into the furnace which was already set at some fixed temperature. The temperature of furnace was between 700°C and 850°C for pure specimen, and between 650°C and 850°C for eutectic additive specimen. The dimensional change ($\Delta L/L_o$) vs time (min.) was measured by the LVDT and recorded on a chart recorder. Only pure MgF_2 and 1 wt.% CaF_2 + 99 wt.% MgF_2 mixed powder specimens were used here.

G. Microstructure Examination :

All specimens were polished and etched by two different solutions : (a) Sulfamic acid[19] (10 gm. of sulfamic acid dissolved in 500 c.c. of H_2O). After etching for 40 min., the specimens were rinsed in alcohol and distilled water.

Only CaF_2 was etched out and MgF_2 was not affected. (b) The polished specimens were etched by concentrated sulfuric and boric acid [20] (100 gm. boric acid in 200 c.c. sulfuric acid) for 7 min. at 150°C. CaF_2 was completely etched out and MgF_2 was also partly etched to reveal the grain boundaries.

The density of specimen before and after sintering was calculated from the linear shrinkage. The density of MgF_2 is taken as 3.1766 gm/cm^3 [21] and the density of CaF_2 is taken as 3.18 gm/cm^3 [22].

The phase diagram of CaF_2-MgF_2 is shown in Fig. 3. [13] with the eutectic temperature at 980°C and a eutectic composition of 55.6 wt.% CaF_2. The dashed line shown on either side along the eutectic temperature indicates uncertainty about the solubility of CaF_2 in MgF_2 and of MgF_2 in CaF_2.

H. Diffusion Experiment :

A MgF_2 single crystal was embedded in CaF_2 powder and heated in vacuum at 950°C for 96 hours. After cooling, the MgF_2 single crystal was removed from the CaF_2 powder. The CaF_2 powder was removed from the surface by a very brief mechanical polish and a depth profile of Ca^{2+} was obtained by SIMS (Secondary Ion Mass Spectroscopy) with Ar ion sputtering at a rate of $\simeq$ 400 Å/ min., and with an ion beam size of 100 μm..

I. Auger Analysis :

The fracture surfaces of 1 wt.% CaF_2 eutectic additive specimen sintered by CHR method at a heating rate of 4.5°C/min. up to 900°C were examined by Auger analysis.

The sensitivity factor in Auger analysis of Ca is 0.47 and of F is 0.48. Since the sensitivity factors for Ca and F are almost identical, we can use peak to peak values to estimate the Ca concentration changes on the basis of F which is constant in our case. We can choose an intergranular fracture region and use Ar ion to sputter down from this fracture surface at a fixed sputtering rate. By comparing the peak to peak values of Ca and F after some fixed sputtering time, the Ca concentration profile along the depth from fracture surface, which is grain boundary in this case, can be obtained.

III. RESULTS and DISCUSSION :

A. Materials :

Upon close examination, it was found that the MgF_2 powder actually consisted of agglomerates composed of MgF_2 crystalites about 0.5 μm in size. Thus, the particle size after classification was actually the agglomerate size (Fig. 4b,c.). The density of pure and additive containing specimens after cold pressing were both 55% theoretical density. There was about 10 wt.% loss after calcination in vacuum at 350°C for 1 hour. From the thermobalance experiments described in section II, the total weight loss was completed below 300°C, which was much lower than the thermal decomposition temperature of $MgCO_3$ (550°C) [23,24,25] and the dehydration of $Mg(OH)_2$ (350°C) [26]. It can be seen that only water evaporation can explain this weight loss. The density of the specimen after calcining was about 57% theoretical density. The slight increase in density is due to contraction of the specimen after losing water located between particles. MgF_2 will react with oxygen and water to form oxides [27].

$$MgF_2 + H_2O \rightarrow MgO + 2HF \qquad \Delta H = 44 \frac{kcal}{mol} \qquad \langle 11 \rangle$$

Therefore, these materials cannot be sintered in oxi-

dizing atmosphere and the water in MgF_2 raw powder must be removed without causing hydrolysis of fluoride.

B. Arrested Zone Sintering :

(a) High temperature portion ($T > 900^{\circ}C$) :

Some workers [17, 28 to 33] have analyzed sintering by using CHR methods. However, the as received raw powder consisted of agglomerates composed of small particles with a size of about 0.2 μm. The powder, after air classification, actually consisted of agglomerates with a size of between 2.5 μm to 10 μm (Fig. 4b,c). It was difficult to get information on the particle size effect on densification since the raw powder only had one uniform, fine particle size. Due to this very fine particle size of the raw powder, the sintering rates were very fast. Very fast heating rates are needed to observe the heating rate effect on the sintering rate. However, the heating rates were limited by the following factors : (a) the large heat capacity of the furnace, (b) the temperature gradient in the specimen, and (c) the instability of the LVDT system caused by large temperature gradients during fast heating. Because of these limitations, neither the heating rate effect nor the particle size influence could be adequately examined.

The microstructures of both pure and 7.6 wt.% CaF_2 additive specimens at $T > 900^{\circ}C$ are shown in Fig. 9 a-d and

A-D.. The specimens were etched in sulfamic acid [34], so that only CaF_2 was attacked. The MgF_2 was not etched by this solution, so in pure MgF_2 specimens as shown in Fig. 9. a-d, the grain boundaries are not revealed. But CaF_2 can be etched out easily to reveal it's location in 7.6 wt.% CaF_2 additive specimens (light gray regions) as shown in Fig. 9. A-D.. The dark gray regions were MgF_2 grains and the black regions were pores. The temperature was determined from the location of the specimen in the furnace. It can be seen that as temperature is raised toward the eutectic temperature, the CaF_2 enriched regions (light gray), which were isolated, became larger in size but smaller in number. When the temperature reached 998°C (Fig. 9C), regions appeared in the polished section where the CaF_2 had been etched out from between the grain, and the MgF_2 grain corners now appeared rounded. This would indicate that the eutectic liquid had formed. The large MgF_2 grains and the morphology of the CaF_2 phase shown in Fig. 9D. suggested that rapid grain growth, characteristic of liquid phase sintered ceramics, had occurred. In order to examine the microstructure of pure MgF_2, another etching solution, concentrated sulfuric and boric acid [20], was used. This solution will strongly attack CaF_2 and etch MgF_2 as well. The dark region in Fig. 10a to d and A to D may therefore be pores or CaF_2. However, the MgF_2 grain structure is revealed clearly by this etchant.

The average grain size for both pure and eutectic

additive containing samples were determined from the number of intercepts of grain boundaries with random straight lines drawn on micrographs (Table 2.). It can be seen from this table that as the temperature is raised from 938°C to 1022°C, the grain size of pure MgF_2 has increased five fold (1 μm to 5 μm from Table 2.), while the grain size for the CaF_2 containing MgF_2 has increased ten fold (2.5 μm to 25 μm from Table 2.).

The linear shrinkage curves and average grain sizes are shown in Fig. 11. The shrinkage rate was obtained by two methods : (a) measured by LVDT, and (b) measured by the local dimensional change before and after AZS. Only (a) has been shown in Fig. 11.. The data of (a) and (b) were in good agreement, except above 1000°C. The discrepancy arises since at T > 1000°C, the grains were extremely large, causing the specimen to crack upon quenching to room temperature. The LVDT method provides more accurate data. Fig. 11. shows that the addition of 7.6 wt.% CaF_2 has greatly enhanced the sintering rate of pure MgF_2 below eutectic temperature (980°C). The additive specimen reached it's final density around 930°C which was 80°C lower than the pure specimen (1010°C).

The rapid apparent shrinkage above 1000°C of the 7.6 wt.% CaF_2 containing specimen (Fig. 11.) was due to the formation of the eutectic liquid, dissolving the intergranular bridges so that the specimen became mechanically very weak

and deformed rapidly under the low stress exerted by dilatometer.

(b) Low temperature portion ($T < 900^{o}C$) :

In this part, pure MgF_2 and 5 wt.% CaF_2 + 95 wt.% MgF_2 specimens were used and the same procedure was followed as described in section II-B. The samples were etched with concentrated sulfuric and boric acid, the microstructures have been shown in Fig. 12a-c and A-C for pure and for CaF_2 containing MgF_2 specimen. The average grain size and corresponding temperature have been shown in Table 3 (from Fig. 12.). The particle size of pure MgF_2 stayed between 0.5 μm to 0.65 μm from 791 ^{o}C to 899 ^{o}C. However, for the CaF_2 containing specimen, the particle size increased four fold from 0.5 μm to 2 μm between 791 ^{o}C to 899 ^{o}C. This indicates that CaF_2 enhanced the mass transport rates of MgF_2 below the eutectic temperature. The grain size and the corresponding shrinkage rates have been shown in Fig. 13. It can be seen from Fig. 11. that rapid grain growth of pure MgF_2 started at about 920 ^{o}C. For the CaF_2-containing specimen, rapid grain growth started at about 850 ^{o}C (Fig. 13.). This roughly corresponds to the temperature at which the densification rates are maximum (from Fig. 11,13.).

Fig. 13. shows the linear shrinkage vs temperature curve which was obtained by two methods : (a) from dilatometric measurements and; (b) from the dimensional changes before and after sintering. Again the additive effect became

detectable as low as 780°C, which is 200°C below the eutectic temperature and the 5 wt.% CaF_2 additive specimen reached its final density around 920°C, which is 100°C lower than that of the pure one (1020°C). There was no measurable difference between pure and additive specimen at temperatures below 780°C.

C. Verification of the Eutectic Temperature of MgF_2-CaF_2 System :

In order to make sure that the additive effect is indeed due to an enhancement of solid state diffusion, a simple experiment was conducted to determined the eutectic temperature of MgF_2-CaF_2 system under the present experimental conditions. The procedure was described in section II-D. The result is shown in Fig. 14. There was a drastic dimensional change at 975°C which indicated that the eutectic liquid had formed at this temperature.

The procedure of eutectic-oxides mixture experiment was also described in section II-D. The results (Fig. 15.) show that both mixtures have only one liquid formed at about 970°C. This indicates that either the oxides did not supress the eutectic temperature or some other liquid did not form below 970°C.

From above, it can be seen that the CaF_2 additive does

enhance the solid state mass transport of MgF_2 below the eutectic temperature.

D. Constant Heating Rate Sintering (CHR) :

Although arrested zone sintering did show the microstructural evolution of pure and eutectic additive specimen, the shrinkage data obtained were not accurate enough due to the fast heating rate between 500°C and 800°C (35°C/min. to 70°C/ min. in Fig. 8.). In addition, the nonlinear heating rate did not premit quantitative analysis. In order to overcome these difficulties, a programmable temperature controller was used for the furnace. Three heating rates, 4.5°C/min., 9°C/min. and 16°C/min., were used. However, the shrinkage data at these heating rates showed little detectable difference. There were two possible reasons for this lack of difference : (a) The primary particle size ($\simeq$ 0.5 μm) was too fine so that a heating rate well above 16°C/min. would have been necessary to introduce the heating rate effect. Unfortunately, controlled linear heating rates in excess of 16°C/min. could not be obtained under the present experimental set-up. (b) The shrinkage rate was strongly temperature dependent and weakly heating rate dependent.

No size effect could be detected since the primary particle size of MgF_2 could not be varied. The experiments

reported in this section only concentrate on the additive effects and microstructure at different temperature for specimen heated at 4.5°C/min. The shrinkage of different CaF_2 containing samples sintered at 4.5°C/min. are shown in Fig. 16A, and the more detailed shrinkage curves and grain size vs temperature curves for different eutectic additive have been shown in Fig. 16B. It can be seen that the sintering rate increases as the additive amount increases, but this effect saturates when the additive concentration becomes greater than 1 wt.% CaF_2. Again little enhancement due to CaF_2 addition could be detected below 700°C. The shrinkage rates vs temperature are shown in Fig. 17. The maximum sintering rates of pure, 0.1 wt.% CaF_2, 1 wt.% CaF_2 and 5 wt.% CaF_2 containing specimens occured at 980°C, 935°C, 890°C and 890°C respectively. This also demonstrates that the enhancement of the eutectic additive effect on sintering rate saturated at about 1 wt.% CaF_2. The microstructures of each composition at 800°C, 900°C and 1000°C were obtained by heating the specimen at 4.5°C/min. to that temperature and quenching it by quickly withdrawing it from the furnace; they are shown in Fig. 18 to 23. The observations at 1000°C, 900°C and 800°C are discussed below.

(a) 1000°C : (Fig. 18, 19)

At this temperature both pure and eutectic additive containing specimens reached their final density (ranging from 89% to 95% of theoretical density), and the final den-

sity increased as the eutectic additive amount increased.

There was exaggerated grain growth in pure MgF_2 and in specimen with 0.1 wt.% CaF_2 (Fig. 18a,b). For 1 wt.% CaF_2 (Fig. 18c) the grain size was much more uniform. This indicated that the grain boundary migration was hindered by 1 wt.% CaF_2 but not by 0.1 wt.% CaF_2.

The eutectic liquid contains 53.3 wt.% CaF_2 (Fig. 3.). Assuming that the eutectic liquid has the same density as MgF_2 and CaF_2, and negelecting solubility of CaF_2 in MgF_2 solid, then the eutectic liquid volume contents for 0.1 wt.% CaF_2, 1 wt.% CaF_2 and 5 wt.% CaF_2 are 0.2%, 1.9% and 9.4% by volume, respectively. From the above assumptions and volume conservation, the liquid film thickness could be calculated approximately :

$$A = \frac{3r^2h}{(r+h)^3}$$

where A is the volume fraction of liquid, r is the radius of the grains, and h is the thickness of the liquid film. For $h \ll r$, $A \simeq 3h/r$, then

$$h = \frac{Ar}{3}$$

From Fig. 18. and Table 4., the grain sizes of 0.1 wt.%, 1 wt.% and 5 wt.% were 10 μm , 20 μm , and 50 μm respectively. Then, the liquid film thickness would be about 30 A, 600 A and 7500 A for 0.1 wt.% , 1 wt.% and 5 wt.%. If there was some finite solubility of CaF_2 in MgF_2

or some voids in the specimen were the eutectic liquid collected, then the actual liquid film thickness would be even smaller. The mass transport rate through a liquid film is proportional to the product of the diffusion coefficient in the liquid (D_l) and liquid film thickness (h). The grain growth rate is proportional to the mass transport rate through liquid film thus proportional to the product of diffusion coefficient in the liquid (D_l) and the liquid film thickness (h). If we take D_l as constant, then the grain growth rate should proportional to the liquid film thickness (h). In 0.1 wt.% and 1 wt.% specimen, the eutectic liquid film thickness was not large enough to introduce large grain growth. In comparing the grain structure of the pure MgF_2 and of the 0.1 wt.% eutectic additive specimen, it can be noted that both have similar sharp grain corners and exaggerate irregular grain growth (Fig. 18a,b). This suggests that the grains in the 0.1 wt.% eutectic additive specimen were not fully wetted above the eutectic temperature. For 1 wt.% additive specimen (Fig. 18c), instead of sharp grain triple junctions, rounded corners were observed, indicating the presence of eutectic liquid. This shows that the solubility of CaF_2 in MgF_2 was less than 1 wt.%. When 5 wt.% CaF_2 was added in MgF_2 at 1000°C, the eutectic liquid would occupy 9.4 wt.% of the volume, and the liquid film thickness of 7500 A should be thick enough to provide substantial mass transport for grain growth. Accordingly, the grain size of 5 wt.% CaF_2 (Fig. 18d) had strongly increased.

After cooling, it appeared that in the 5 wt.% CaF_2 specimen, the liquid was not covering the entire boundary. There were some small "neck" regions between grains as shown in Fig. 18d. A larger magnification of such a neck is shown in Fig. 19D. A direct grain boundary appears to be located in the middle of neck. This is probably due to the pressure exterted by LVDT.

(b) 900°C : (Fig. 20,21)

The final densities for both pure MgF_2 and CaF_2 containing MgF_2 quenched from 900°C are shown in Table 5. Again, the trend of a final density increase with increasing additive amount was observed, but the results fall into two categories : (a) 68.3 % and 69.6 % theoretical density for pure and 0.1 wt.%, and (b) 87.4 % and 89.3 % theoretical density for 1 wt.% CaF_2 and 5 wt.% CaF_2. The final densities of these two categories differ greatly. Apparently, 0.1 wt.% CaF_2 additive was not sufficient to enhance the sintering rate of MgF_2 either by enhancing its bulk diffusion rate or by enhancing its grain boundary diffusion rate.

The microstructure of both pure and eutectic additive containing specimens are shown in Fig. 20 and 21. Again, the microstructures fall into two distinguishable groups : (a) pure and 0.1 wt.% CaF_2, (b) 1 wt.% and 5 wt.% CaF_2. In group (a), as shown in Fig. 20a,b, the particle sizes were about 1.2 μm , 2 μm, for pure and 0.1 wt.% CaF_2. The necks between the particles for 0.1 wt.% CaF_2 were larger than

that for the pure one (Fig. 21A,B). Both contained open porosity and low density which indicated that they were still in the early stage of sintering. In group (b) , as shown in Fig. 20c,d and Fig. 21C,D, the grain sizes were about 3 μm for both 1 wt.% and 5 wt.% CaF_2. Both samples exhibit closed porosity and a high density which indicated that they had already reached the final sintering stage. From these observations it can be concluded that 1 wt.% CaF_2 was sufficient to fully enhance the sintering rate of MgF_2 below eutectic temperature. More than 1 wt.% CaF_2 addition does not contribute in further enhancing the sintering rate.

(c) 800°C : (Fig. 22 and 23)

The particle sizes at this temperature were found to be about 0.5 μm for both pure and additive containing specimen. The microstructure revealed open porosity, and the density remained low (60 % to 63 % theoretical density, see Table 5). This indicated that all specimens were still in the early sintering stage. However, the CaF_2 additive did increase the size of contact region between two grains and appeared to lead to a surface smoothing of the particles. Especially for 1 wt.% and 5 wt.% CaF_2, the contact regions were very large compared to pure MgF_2, about 0.5 μm for 1 wt.% and 5 wt.% CaF_2 additive and 0.2 μm for pure MgF_2 (Fig. 23A,C,D). Also, 0.1 wt.% CaF_2 had increased the neck sizes to about 0.3 μm (Fig. 23B).

E. Constant Temperature Sintering (CTS) :

From the above experiments, it could be concluded that the addition of CaF_2 to MgF_2 greatly increases the solid state mass transport rate below the eutectic temperature, where eutectic liquid phases are not present. However, the mechanisms that cause the increasing densification rate below eutectic temperature need to be examined further. The first approach was to use the CTS experiments to determine the apparent activation energy Q, and the time exponent n in Eq. <6> to see which mechanism might dominate.

Since this method is not very reliable if surface diffusion was important, a second approach was to make a reasonable estimate about which diffusion mechanism is possible, by comparing the a diffusion coefficient from CTS experiment to that from diffusion experiment.

From CTS experiment and Johnson's equations (16) (Eq.<7>,<8>) we can estimate the diffusion coefficient necessary to contribute to the observed densification rate of the specimen and can compare that to the diffusion coefficient estimated from diffusion experiment. Let us decribe the first method as follow :

If the CTS data are plotted in a logarithm shrinkage - logarithm time plots, the shrinkage curves apeared to straighten after an initial curvature, and the slopes of the "straight" part of the curves were lower than 0.33. This can

not be interpreted by any model [35 to 37]. Further analysis of the data showed that the low slopes of the "straight" part of the curves and the initial curvature could arise if systematic errors in $\Delta L/L_o$ and t(min.) were present. Such errors could be attributed to the rapid sintering of very fine MgF_2 powder before reaching temperature equilibrium. Errors in shrinkage and time can be assessed by plotting the length at any time, L, as a function of t^n, where n is chosen as either 0.33 for grain boundary diffusion or 0.46 for volume diffusion [37]. Each set of data can then be made to fit into a linear $\log \Delta L/L_o$ - log t relationship by subtraction of a time correction, δt, from the time at each point on the curve. When the data were thus fitted , it was found that the extrapolated length at $t - \delta t = 0$, L_e, was less than the initial length of each compact. This, in effect, expresses the fact that some densification had taken place before temperature equilibrium had been reached.

The values of δt and L_e have been shown in Table 6. It can be seen from this table that δt was about 5 min. in all cases, a reasonable time for the system to reach temperature equilibrium. The data for 1 wt.% CaF_2 at temperatures above 790°C can not be fitted with n = 0.33, instead, they fit well when n is put equal to 0.46, as appropriate for a bulk diffusion transport mechanism [37].

The data were thus plotted with a corrected time log $(t-\delta t)$ vs corrected length log $(\Delta L/L_e)$. The curve for pure

and 1 wt.% CaF_2 additive specimen is shown in Fig. 24,25. The slopes of these curves are the exponent n in Eq. <2>. Here $n \simeq 0.33$ for the data below 750°C of the 1 wt.% CaF_2 containing specimens. Above 750°C the slope of 1 wt.% CaF_2 containing MgF_2 changed to $n \simeq 0.46$. For the pure MgF_2, the slope $n \simeq 0.46$ between 706°C and 841°C. The deviation from a straight line at higher shrinkage is caused by the breakdown of the model when the compact enters the final sintering stage.

Log k_q as a function of $1/T$ (K^{-1}) is shown in Fig. 25. , where k_q (see Eq. <6>) was defined as the evaluation of log $(\Delta L/L_o)$ at log $(t-\delta t)=0$ plus n log T (Fig. 24,25.). The slope of line is equal to $nQ/2.302R$ where R is gas constant. The apparent activation energy for pure MgF_2 in the range of 706°C to 841°C is found to be 56 kcal/mol and corresponded to volume diffusion mechanism from the value of $n \simeq 0.46$. For the additive specimen, when the temperature was below 750°C, the apparent activation energy was 36 kcal/mol for a grain boundary diffusion mechanism (from the value of $n \simeq 0.33$), but when the temperature was above 750°C and up to 848°C, it appeared that a volume diffusion mechanism would dominate (from the value of $n \simeq 0.46$) with an apparent activation energy of 64 kcal/mol.

The above results (from the values of n) show that a volume diffusion mechanism would dominate for the pure MgF_2 from 706°C to 841°C, while for the 1 wt.% CaF_2 additive

specimen a volume diffusion mechanism would dominate from 750°C to 848°C, and a grain boundary diffusion mechanism would dominate from 670°C to 750°C. However, as discussed in section I, Johnson [18] pointed out that this method was not reliable if surface diffusion plays an important role. Thus in order to conclude that either a volume diffusion or a grain boundary diffusion mechanism was dominant, it is necessary to compare the diffusivity needed to account for the observed shrinkage during CTS experiment to that obtained from the diffusion experiment.

F. Diffusion Experiment :

From Fig. 27. it can be seen that Ca^{2+} did diffuse into the MgF_2 single crystal bulk. From sputtering rate and time, the approximate diffusion depth s can be estimated as 1 μm, and using Eq. <9>., the diffusion coefficient of Ca^{2+} in MgF_2 single crystal at 950°C is estimated to be 2.894×10^{-14} cm^2/sec.

In order to calculate the diffusion coefficient at some other temperature, Eq. <10> leads to

$$\frac{D_a}{D_b} = \exp\left(-\frac{Q}{R}\left(\frac{1}{T_a} - \frac{1}{T_b}\right)\right)$$

$$D_a = D_b \exp\left(-\frac{Q}{R}\left(\frac{1}{T_a} - \frac{1}{T_b}\right)\right) \qquad <17>$$

where D_a = diffusion coefficient at temperature T_a; D_b

= diffusion coefficient at temperature T_b; Q = activation energy for the diffusion process; R = gas constant.

D_b and T_b were known from the diffusion experiment; Q needs to be known in order to calculate D_a at T_a. Unfortunately, the activation energy Q was not available from the literature and therefore needs to be estimated. Cooper and Heasley [38] have developed an expression for the interdiffusion coefficient in a binary system consisting of two cations and a common anion, i.e.

$$D = \frac{Z_2N_{23}D_1(Z_3D_3 - Z_2D_2) + Z_1N_{13}D_2(Z_3D_3 - Z_1D_1)}{Z_1Z_3N_{13}D_3 - Z_1^2N_{13}D_1 + Z_2Z_3N_{23}D_3 - Z_2^2N_{23}D_2}\left(1 + \frac{d\ln\gamma_{13}}{d\ln N_{13}}\right) \quad \langle 18 \rangle$$

where Z_i represents the valence of the ith ion; subscripts 1, 2 and 3 represent the two cations and the common anion, repectively; N_{13} and N_{23} are mole fractions of the two end-member compounds in the solution at the particular composition under consideration; and γ_{13} is the activity coefficient for component 13 in the solution.

In the CaF_2-MgF_2 system, $Z_1 = Z_2 = +2$, $Z_3 = -1$ and D_1, $D_2 \ll D_F$, since in the fluorite structure, diffusivities for anions are orders of magnitude greater than those for cations [34]. Eq. <18>, thus simplifies to

$$D = (N_{13}D_2 + N_{23}D_1)\left(1 + \frac{d\ln\gamma_{13}}{d\ln N_{13}}\right) \quad \langle 19 \rangle$$

Letting N_{13} and N_{23} represent mole fraction of CaF_2 and

MgF_2, respectively, and making the reasonable assumption that Ca^{2+} and Mg^{2+} substitute ideally for each other at infinite dilution, Eq. <19> gives the result that, at $N_{13} \simeq 0$, i.e. in nealy pure MgF_2,

$$D \simeq D_{Ca}$$

and, at $N_{13} \simeq 1$, i.e. nearly pure CaF_2,

$$D \simeq D_{Mg}$$

This result suggests that the values of D extrapolated to the extremes of composition should be directly comparably with tracer-impurity diffusion coefficients measured in the nearly pure materials. Some interdiffusion activation energy in alkaline-earth fluorides were shown in Table. 7.. The average volume occupied by MgF_2 (33.44 $Å^3$) is smaller than that occupied by CaF_2 (40.47 $Å^3$). It would be expected that Ca^{+2} ion moves more easily through the more expanded CaF_2 structure than through the more constricted MgF_2 sturcture. From above, we can reasonably assume that the activation energy for Ca^{+2} diffusion into MgF_2 single crystal would be at least on the order of the activation energy of Ca^{+2} in CaF_2 single crystal, i.e. 95.7 kcal/mol. Thus the volume diffusivity of Ca^{+2} in MgF_2 can be estimated from Eq. <17> and the results were shown in Table 8.

G. Diffusivity Calculation :

The diffusivity necessary to contribute to the shrinkage of specimen was calculated by using Eq. <7>,<8>. If volume diffusion dominates, the volume diffusion coefficient can be calculated from Eq. <7> (D_{sv} in Table 8.). If grain boundary diffusion dominates, the grain boundary diffusion coefficent (D_{sb} in Table 9.) times grain boundary width (b) can be calculated from Eq. <8>. Before using Eq. <7> and <8> some variables must be first reasonably estimated.

(1) Surface energy : Take γ = 500 ergs/cm^2 in this calculation.

(2) Vacancy volume : Since the cation is assumed to be the slower diffusion species in flourides [34], the vacancy volume can be calculated from following equation [35] :

$$\delta^3 = \frac{\text{molar weight}}{1 \text{ X density X N}} \qquad <20>$$

$$= \frac{62.31}{1 \text{ X } 3.1766 \text{ X } 6.02\text{X}10^{23}}$$

$$= 3.27 \text{ X } 10^{-23} \text{ cm}^3$$

If flourines were slower, the value of δ^3 should be divided by 2, since when two ions of the slower diffusion species have deposited, there will be one molecular volume change.

(3) Particle size : Using r = 0.5 μm = 5 X 10^{-5} cm in here.

(4) Shrinkage y at sintering time t (sec) and sintering temperature (K) were obtained in the CTS experiment. The y values of experiment at three different temperatures for 1 wt.% CaF_2 additive in CTS experiment were used.

The volume diffusion coefficient and grain boundary diffusion coefficient calculated from Eq. <7> or Eq. <8> were given in Table 8,9..

It clearly can be seen from Table 8,9. that the volume diffusion coefficients calculated from diffusion experiment were about 10^{-3} lower than those calculated from sintering data. If we take the grain boundary width b = 10^{-7} cm and D_b to be 10^4 times D_v at the same temperature, a not unusual ratio, it can be seen that the two grain boundary diffusion coefficients can be made fit quite well (Table 9.).

The apparent activation energies obtained from log k_q vs log 1/T curve in n=0.46 region were 56 kcal/mol for pure MgF_2 (706°C to 841°C) and were 64 kcal/mol for 1 wt.% CaF_2 additive speicmen (750°C to 848°C), both are too low compared to the bulk diffusion activation energy (95.7 kcal/mol or higher) expected from Eq. <17>.

Short and Roy [39] reported that the activation energy for Ca^{+2} diffusing in polycrystalline CaF_2 was 39.2 kcal/mol (1.7 ev). This value can be taken as the lower limit for the

grain boundary diffusion activation energy and compared it to the activation energy (36 kcal/mol) obtained from the log k_q vs log 1/T curve for 1 wt.% CaF_2 additive in n=0.33 region (670°C to 750°C). The agreement is reasonable.

Coble [35] mentioned that within the limits of solid solubility, different solubilities at the boundaries would then require that the solute gradient be moved with the moving boundary. Grain boundary migration would exhibit kinetics typical of bulk rather than boundary processes. This can explain the volume diffusion slope of the high temperature region of 1 wt.% CaF_2 additive (750°C to 848°C).

From the above disscusions, it can be concluded that the effect of the CaF_2 eutectic additive was to fully enhance the grain boundary diffusion rate rather than volume diffusion rate, since the volume diffusion coefficient was too low to account for the shrinkage obtained from CTS experiment. In addition, the activation energy obtained from the CTS experiment was too low to compare to the volume diffusion activation energy.

How the CaF_2 enhances the grain boundary diffusion rate of MgF_2 still remained unclearly. However, from the phase diagram (Fig. 3.) the homologeous temperature, i.e. temperature divided by its melting temperature (in K), at the maximum shrinkage rate for pure MgF_2 was 0.82 (at 980°C in Fig. 17.). If we take the melting temperature of 1 wt.% CaF_2 additive specimen to be the eutectic temperature (980°C),

then the homologeous temperature for the CaF_2 enriched grain boundary at this maximum shrinkage rate (at 890°C in Fig. 17.) was 0.93. That would mean that the CaF_2 additive, accumulated at the grain boundary of MgF_2 forms a chemically altered layer which may provide a high diffusion path for MgF_2. It could be considered that the eutectic additive concentration lowered the grain boundary melting temperature of the pure specimen to the eutectic temperature. Strongly enhanced grain boundary transport would then be expected without the presence of a physical liquid phase.

IV. CONCLUSIONS :

Pre-eutectic densification phenomena has been studied. The results show that the sintering rate of MgF_2 was enhanced by CaF_2 eutectic additive, and that the effectness of CaF_2 saturates at about 1 wt. %. The enhancement of sintering rate started about 200°C below the eutectic temperature. The eutectic temperature of CaF_2 - MgF_2 system in our experimental condition has been verified to be about 975°C. By mixing eutectic composition of CaF_2 - MgF_2 with CaO and MgO, it was shown that no liquids formed below 970°C. In addition, no liquid phase etching patterns which rounded grain corners were found below 980°C. This indicates that the eutectic additive enhances the solid state mass transport of MgF_2.

The volume diffusivity obtained from diffusion experiment was about three orders of magnitude lower than that obtained from CTS experiment. This indicates that a volume diffusion mechanism is not plausible. By making reasonable assumptions, the grain boundary diffusivities obtained from both experiments can be made to agree well. Auger analysis on fracture surface of specimen which was sintered by CHR method up to 900°C at 1 wt.% eutectic additive, showed a strong enhancement of Ca on grain boundaries, in a region of thickness $\simeq$ 100 Å.

It is concluded that pre-eutectic densification kinet-

ics result from increase grain boundary transport due to the presence of the eutectic forming additive.

ACKNOWLEDGEMENT

I wish to express my gratitude to professor L.C. De Jonghe for his continuous encouragement and support while conducting this research. I am also grateful to professor A. G. Evans and D. P. Whittle for their enlightening discussions and critical review of the manuscript.

The help of my fellow graduate students throughout this work is greatly acknowledged. Further thanks are extended to K. A. Gaugler and Gloria Pelatowski for their technical assistance.

Research facilities and technical staff were provided by the U. S. Department of energy through the Materials and Molecular Research Division of the Lawrence Berkeley Laboratory, under Contract No. W-7405-ENG-48.

Finally I would like to express special thanks to my parents and my wife Hsien-Hsien for their continuous love, encouragement and support.

Table 1.

Mass spectrographic analysis data of MgF_2 from Materials Research Corporation.

Typical Analysis	
Element	ppm
Si	50
Pb	10
Cu	1
Ni	10
Co	10
Mn	10
Cr	10
Ca	100
Li	50
Na	30

Table 2.

The average grain size of pure and 7.6 wt.% CaF_2 additive in MgF_2, sintered by the arrested zone sintering at 0.2"/min. feeding rate. Also shown in Fig. 9,10.

Temp. ^oC	Pure MgF_2 G.S. (μm)	7.6 wt.% CaF_2 G.S. (μm)
938	1	2.5
969	1.5	3
998	4	6
1022	5	25

Table 3.

The average grain size for pure and 5 wt.% CaF_2 additive in MgF_2, sintered by AZS at 0.2"/min. feeding rate. Also shown in Fig. 12.

Temp. ^oC	Pure MgF_2 G.S. (μm)	5 wt.% CaF_2 G.S. (μm)
791	0.5	0.5
852	0.5	0.7
899	0.65	2.0

Table 4.

The grain size of pure and additive specimen, sintered at 4.5°C/min. to 800°C , 900°C and 1000°C..

Temp. °C	Additive (wt.% CaF_2)	Grain size(μm)
800	0	0.4
800	0.1	0.5
800	1	0.5
800	5	0.5
900	0	0.6
900	0.1	1.0
900	1	2.2
900	5	2.4
1000	0	10
1000	0.1	10
1000	1	20
1000	5	50

Table 5.

The final densities of pure and additive samples at 1000°C, 900°C and 800°C, sintered by CHR at 4.5°C/min. Also shown in Fig. 17 to 22.

Additive wt.% of CaF_2	Temp. °C	Final Density g/cm^3	Theoretic Density %
0	1000	2.8	89.0
0.1	1000	2.9	91.9
1	1000	3.0	93.4
5	1000	3.0	95.8
0	900	2.2	68.3
0.1	900	2.2	69.6
1	900	2.8	87.5
5	900	2.8	89.3
0	800	1.9	60.4
0.1	800	1.8	57.8
1	800	2.0	63.2
5	800	2.0	63.9

Table 6.

The slope n, time correction δt (min.) and extrapolated length at $t - \delta t = 0$, L_e of pure and 1 wt.% CaF_2 additive in MgF_2 specimen at different temperature by contanst temperature sintering method.

Additive wt.% of CaF_2	Temp. ^oC	n	δt (min.)	L_e (mil.)
0%	706	0.46	5.5	149.0
	746	0.46	5	138.4
	778	0.46	5.5	144.1
	794	0.46	4.5	144.8
	841	0.46	6	145.5
1%	670	0.33	5.5	146.4
	706	0.33	5	151.3
	747	0.33	5	147.1
	790	0.46	5.5	144.5
	823	0.46	5	143.9
	848	0.46	5	141

Table 7.

Some interdiffusion or self-diffusion activation energies of alkaline- earth fluorides.

Diffusion Ion	Matrix	Q(kcal/mole)	Ref. No.
Sr	CaF_2	100.8	40
Sr	SrF_2	99.2	40
Sr	BaF_2	86.5	40
Ca	CaF_2	95.7	39
Sr	CaF_2	101	39
Ca	SrF_2	89.6	39
Sr	SrF_2	99.2	39
Ca	CaF_2 (Polycrystal)	39.2	40

Table 8.

Volume diffusion coefficient calculated from (a) Diffusion experiment (D_d). (b) CTS experiment (D_s).

Temperature	D_{dv}	D_{sv}
^oC	$cm^2/sec.$	
950	2.89×10^{-14}	
823	3.01×10^{-16}	6.13×10^{-13}
790	7.69×10^{-17}	2.02×10^{-13}
747	1.14×10^{-17}	1.64×10^{-14}

Table 9.

Grain boundary diffusion coefficient calculated from (a) Diffusion experiment (D_d). (b) CTS experiment (D_s).

Temperature	D_{db}	bD_{sb}	D_{sb}
^oC	cm^2/sec	cm^3/sec	cm^2/sec
950	2.89×10^{-14}		
823	3.01×10^{-12}	2.32×10^{-18}	2.32×10^{-11}
790	7.69×10^{-13}	5.43×10^{-19}	5.43×10^{-12}
747	1.14×10^{-13}	3.06×10^{-20}	3.06×10^{-13}

REFERENCES :

1. L.C. De Jonghe and Edward Goo. in Process. of crystalline Ceram. Materials Science Research. 11, p433 (1978).

2. L.C. De Jonghe and H. Chandan, Ceram. Bull., 55, [3], p312, (1976).

3. L.C. De Jonghe and H. Chandan, U.S. Patent 3,959,022, May, 25, (1976).

4. S. Weiner, Ford Motor Company, RANN, NSF-C805 (AER-73-07199), Jan. (1975).

5. W.D. Kingery, J. App. Phys. 30, [3], p301 (1959).

6. F.V. Lenel, Trans Am. Inst. Mining. Met. Engrs, 175, p878, (1948)

7. J. Gurland and J.T. Norton, J. Metals, p1051, (1952)

8. H.S. Cannon and F.V. Lenel in Plansee Proceedings, (1952), F. Beverorsky, editor (Metalwerk Plansee, Reutee, 1953), p106.

9. G.H. Gessinger and H.F. Fischmeister, J. Less-Common Met., 27, p129 (1972).

10. J.H. Brophy, L.A. Shepard and J. Wulff, Powder Met. Interscience. N.Y., p113 (1961).

11. W. Schintlmeister and K. Richter., Planseeber, Pulvermet., 18, p3 (1970).

12. H.E. Exner, Science of Sintering, Theory and Practice, 6, Supplement p30 (1974).

13. Ernest M. Levin and Howard F. McMurdie, "Phase Diagrams for Ceramists 1975 Supplement" Am. Ceram. Soc. p361, Fig. 4820.

14. W.D. Kingery and M. Berg., J. App. Phys., 26, [10]. p1205 (1955).

15. R.L. Coble, J. Am. Ceram. Soc., 41, [2]. p55 (1958).

16. D.L. Johnson and T.M. Clarke, Acta Met., 12, [10], p1173 (1964).

17. J.J Bacmann and G. Cizeron., J. Am. Ceram. Soc., 51, [4], p209, (1970)

18. D.L. Johnson, "Solid-State Sintering", Chap. 9 in Ultrafine Grain Ceramics, ed. J .J. Burke, N.L. Reed and V. Weiss, Syracuse U. Press, (1970).

19. W.L. Phillps. Jr., J. Am. Ceram. Soc. 44, p499 (1961).

20. Hal H. Rice and Murice J. Garey., Am. Ceram. Soc. Bull. 46, [12], p1149 (1967).

21. Dean A. Buckner, Harold C. Hafner and Norbert J. Kreidl., J. Am. Ceram. Soc., 45, [9], p435 (1962).

22. Eitude Faite à L'Ecole par M. Michel Lacroix, I'INDUSTRIE CERAMIQUE Janvier, [537], p50 (1962).

23. H.T.S. Britton, S.J. Gregg, and G.W. Winsor, "Calcination of Dolomite I," Trans Faraday Soc, 48, p63-69 (1952)

24. L. Bachmann and E. Cremer, " Kinetics of the Thermal Decomposition of Magnesium and Calcium Carbonate" Z. Anorg. Allgem Chem., 309, [1-2], p65-70 (1961).

25. L. Bachmann and E. Cremer ; p147-75 in proceedings of International Symposium on Reactivity of Solids, Madrid, (1956), Vol.III, C. Bermejo, Madrid, (1959).

26. S.J. Gregg and R.I. Razouk, "Kinetics of thermal Decomposition of Magnesium Hydroxide." J. Chem. Soc. (London), (1949), p36-44.

27. M. Bourg et A. Bourg, Vacuum, 14, p253 (1964).

28. J.L. Woolfrey and M.J. Bannister, J. Am. Ceram. Soc., 55, [8], p390 (1972).

29. Ivan B. Cutler, J. Am. Ceram. Soc., 52, [1], p14 (1969).

30. Wyne S. Young and Ivan B. Cutler, J. Am. Ceram. Soc., 53, [12], p659 (1970).

31. D.A. Venkatu and D. Lynn Johnson., J. of Am. Ceram. Soc., 54, p641 (1971).

32. M.J. Bannister, J. Am. Ceram. Soc., 51, [10], p548 (1968).

33. J.L. Woolfrey, J. of Am. Ceram. Soc., 55, [8]. p383 (1972).

34. Ralph Scheidecker and M.F. Berard. J. Am. Ceram. Soc. 56, [4], p204 (1973).

35. R.L. Coble, J. Am. Ceram. Soc., 41, p55 (1958).

36. D.L. Johnson and I.B. Cutler, J. Am. Ceram. Soc. 46, p541 (1963).

37. D. Lynn Johnson, J. App. Phys. 40, [1], p192 (1969).

38. A.R. Cooper, Jr., and J.H. Heasley, J. Amer. Ceram. Soc. 49, [5], p280-84, (1966).

39. Short J. and Roy R., J. Phys. Chem. 68, p3877, (1964).

40. M. Baker and A. Taylor, J. Phys. Chem. Solids. 30, p1003, (1969).

FIGURE CAPTIONS :

Fig. 1. Local shrinkage $\Delta L/L_o$ as a function of position during zone sintering of sodium beta alumina. A : eutectic additive sample; B : additive free sample. The green densities are 60% of the theoretical density. The eutectic temperature is about 1575°C.(XBL 815-9724)

Fig. 2. Configuration for an idealized refractory metal-activated sintering after Gessinger and Fischmeister [9].(XBL 814-5605)

Fig. 3. Phase diagram of CaF_2 and MgF_2 [13].(XBL 8010-12627)

Fig. 4. The MgF_2 powder after classified and CaF_2 powder as received. a. CaF_2, b. MgF_2 (fine powder), c. MgF_2 (coarse powder). (XBB 815-4301)

Fig. 5. Processing diagram for MgF_2 pure and doped CaF_2 powder. (XBL 814-5599)

Fig. 6. A block diagram of the dilatometer set-up. (XBL 815-5663)

Fig. 7. Temperature profile of AZS. (XBL 814-5606)

Fig. 8. Heating rate of temperature profile in Fig. 7. (XBL 814-5622)

Fig. 9. Microstructure of pure (a to d) and 7.6 wt.% CaF_2 (A to D) in MgF_2, sintered by AZS method and etched by sulfamic acid. The location of CaF_2 can be seen clearly (A to D), but the grain boundary of MgF_2 was not shown. The temperatures were : a.A. 938°C, b.B. 969°C, c.C. 998°C, d.D. 1022°C. (XBB 814-3807)

Fig. 10. Microstructure of pure (a to d) and 7.6 wt.% CaF_2 (A to D) in MgF_2, sintered by AZS method and etched by concentrated sulfuric acid and boric acid. The grain boundary of MgF_2 can be seen clearly. The temperatures were : a.A. 938°C, b.B. 969°C, c.C. 998°C, d.D. 1022°C. (XBB 814-3808)

Fig.11 Shrinkage and grain size vs temperature for pure MgF_2 and 7.6 wt.% CaF_2 in MgF_2, sintered by AZS method at 0.2"/min. feeding rate. (XBL 814-5601)

Fig.12. Microstructure of pure and 5 wt.% CaF_2 additive MgF_2 sintered by AZS method and etched by concentrated sulfuric and boric acid. The temperatures were : a.A. 791°C, b.B. 852°C, c.C. 899°C. (XBB 814-3806)

Fig.13. Shrinkage curve and average grain size of pure and 5 wt.% CaF_2 in MgF_2, sintered by AZS method at 0.2"/min. feeding rate. (XBL 814-5600)

Fig.14. Shrinkage curve of MgF_2-CaF_2 diffusion couple, heating up at 4.5°C /min. to 982°C. There was a drastic dimensional change at 975°C. (XBL 814-5602)

Fig.15. The effects of oxides on eutectic temperature of CaF_2 - MgF_2 system. Pure CaF_2 - MgF_2 eutectic mixture and eutectic-oxide mixture powders, which is the eutectic mixture plus 5 wt.% CaO and 5 wt.% MgO, were vacuum calcined 1 hr at 350°C and heated up at 4.5°C/min. to 1000°C. The thermocouples were embedded in these powders and the temperature vs time curve was recorded on a chart recorder. There is no liquid formed below 970°C. (XBL 815-5786)

Fig.16A Shrinkage curve of pure, 0.1 wt.%, 1 wt.% and 5 wt.% CaF_2 in MgF_2 , sintered at 4.5°C/min. heating rate. (XBL 814-5597)

Fig.16B Shrinkage and grain size vs temperature for pure MgF_2, 0.1 wt.%, 1 wt.% and 5 wt.% CaF_2 additive specimen. (XBL 814-5598)

Fig.17. Slope of shrinkage rate vs temperature for 0.1 wt.%, 1 wt.% and 5 wt.% CaF_2 additive MgF_2, sintered at 4.5°C/min. heating rate. (XBL 814-5604)

Fig.18. Microstructure of pure and additive specimen, sintered at 4.5°C/min. heating rate up to 1000°C, etched by concentrated sulfuric and boric acid. (a) Pure MgF_2, (b) 0.1 wt.% CaF_2, (c) 1 wt.% CaF_2, (d)

5 wt.% CaF_2. (XBB 814-3804)

Fig.19. Higher magnification of Fig. 18. (A) pure MgF_2, (B) 0.1 wt.% CaF_2, (C) 1 wt.% CaF_2, (D) 5 wt.% CaF_2. (XBB 814-3800)

Fig.20. Microstructure of pure and additive specimen, sintered at 4.5°C/min. up to 900°C, etched by concentrated sulfuric and boric acid. (a) pure MgF_2, (b) 0.1 wt.%, (c) 1 wt.%, (d) 5 wt.% CaF_2. (XBB 814-3802)

Fig.21. Higher magnification of Fig. 21. (A) Pure MgF_2, (B) 0.1 wt.%, (C) 1 wt.%, (D) 5 wt.% CaF_2. (XBB 814-3801)

Fig.22. Microstructure of pure and additive specimen, sintered at 4.5°C/min. up to 800°C, etched by concentrated sulfuric and boric acid. (a) Pure MgF_2, (b) 0.1 wt.%, (c) 1 wt.%, (d) 5 wt.% CaF_2. (XBB 814-3803)

Fig.23. Higher magnification of Fig. 23. (A) Pure MgF_2, (B) o.1 wt.%, C. 1 wt.%, (D) 5 wt.% CaF_2. (XBB 814-3805)

Fig.24. $\log(t-\delta t)$ vs $\log(\Delta L/L_e)$ for pure MgF_2 specimen sintered by CTS method at different temperatures. The extrapolated line intercepts at x = 0 plus n log T correspond to log k_q. The slope gives the time

exponent n. (XBL 815-5784)

Fig.25. Log(t-δt) vs log($\Delta L/L_e$) for 1 wt.% CaF_2 additive specimen, sintered by CTS method at different temperatures. The slope gives the time exponent n. (XBL 815-5785)

Fig.26. Plot $1/T(^oK)$ vs log k_q from Fig. 25,26. for both pure and 1 wt.% CaF_2 additive specimen. The slope gives -nQ/2.302R from which we can get the apparent activation energy Q by combining Fig. 25,26,27. (XBL 815-5783)

Fig.27. The depth profile of Ca^{+2} in the MgF_2 single crystal, which was embeded in CaF_2 powder and annealed at 950°C for 96 hours, was detected by SIMS (Secondary Ion Mass Spectroscopy) with sputtering rate of 400 Å/min. and ion beam size of 100 μm for 70 min.. (XBL 814-5603)

Fig.28. The Auger electron depth profile on fracture surface of CHR specimen which was 1 wt.% CaF_2 eutectic additive vacuum sintered at 4.5°C/min. up to 900°C. The intergranular region which was enriched with Ca was selected to do Ca depth profile. The Ar ion sputtering rate is approximately 100 Å/min.. The extremly sharp decay of Ca concentration indicates that Ca concentrates at grain boundary with thickness of 100 Å.(XBL 815-5836)

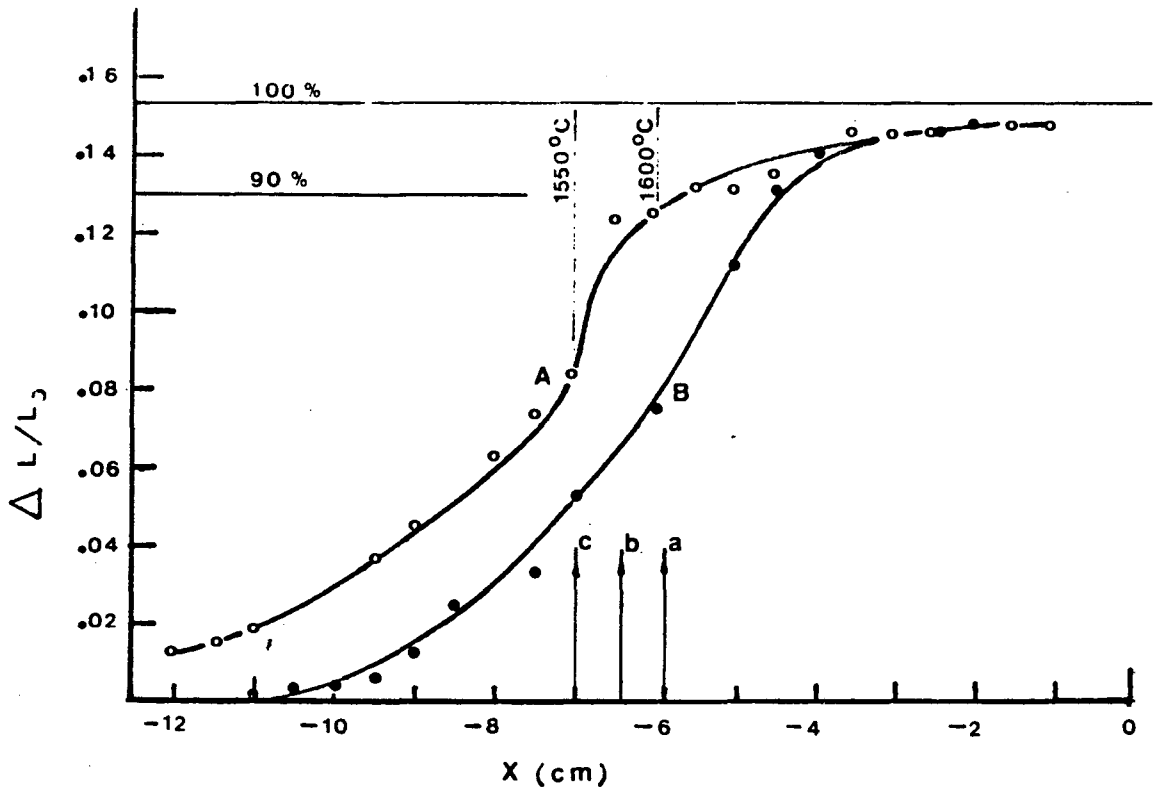

XBL 815-9724

Fig. 1

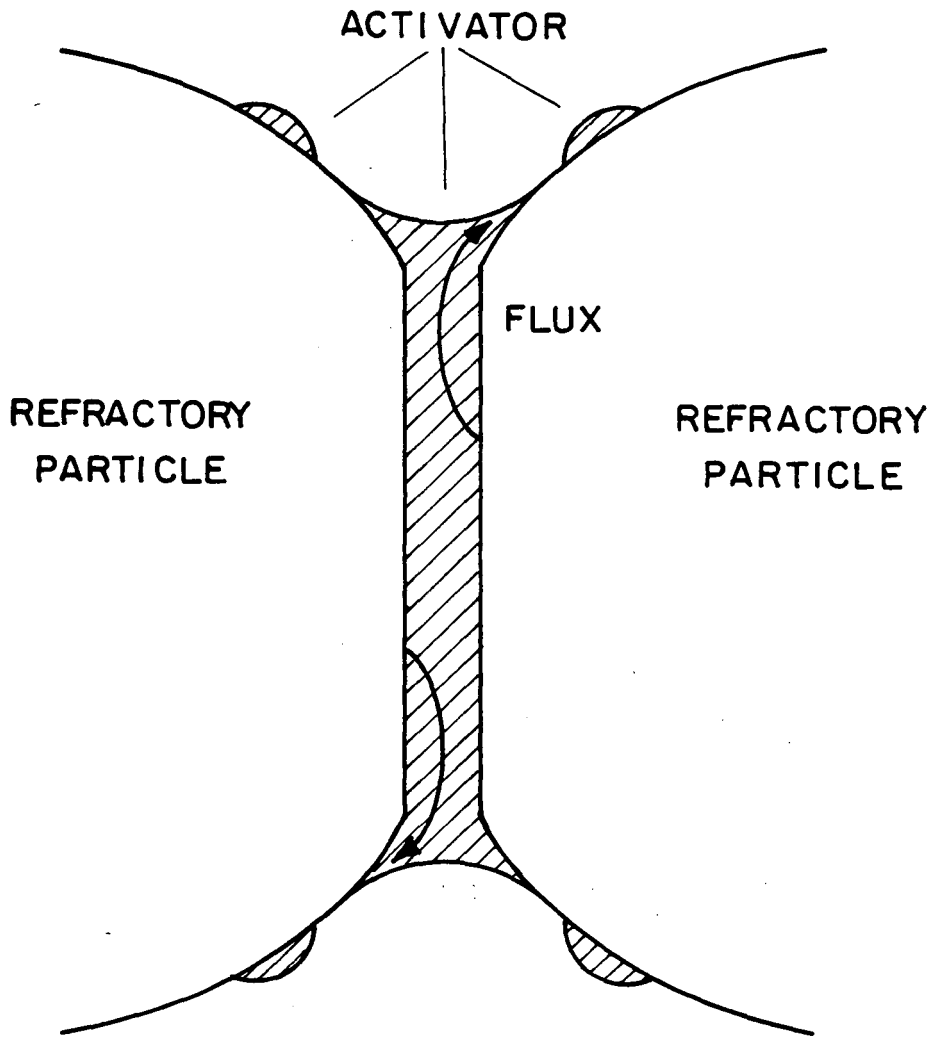
ACTIVATOR
FLUX
REFRACTORY PARTICLE
REFRACTORY PARTICLE
XBL 814-5605

Fig. 2

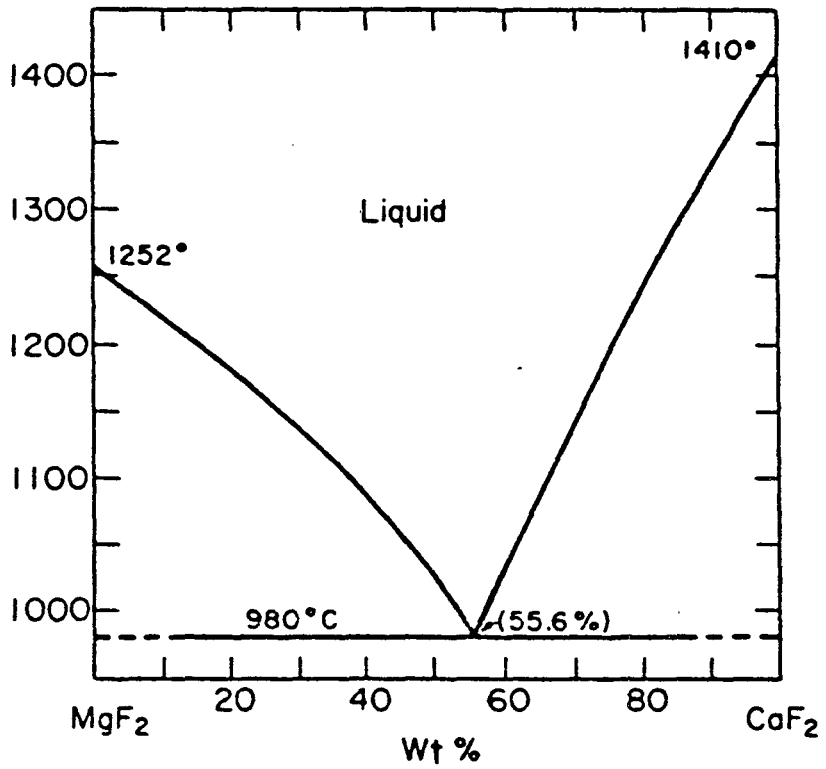

XBL 8010-12627

Fig. 3

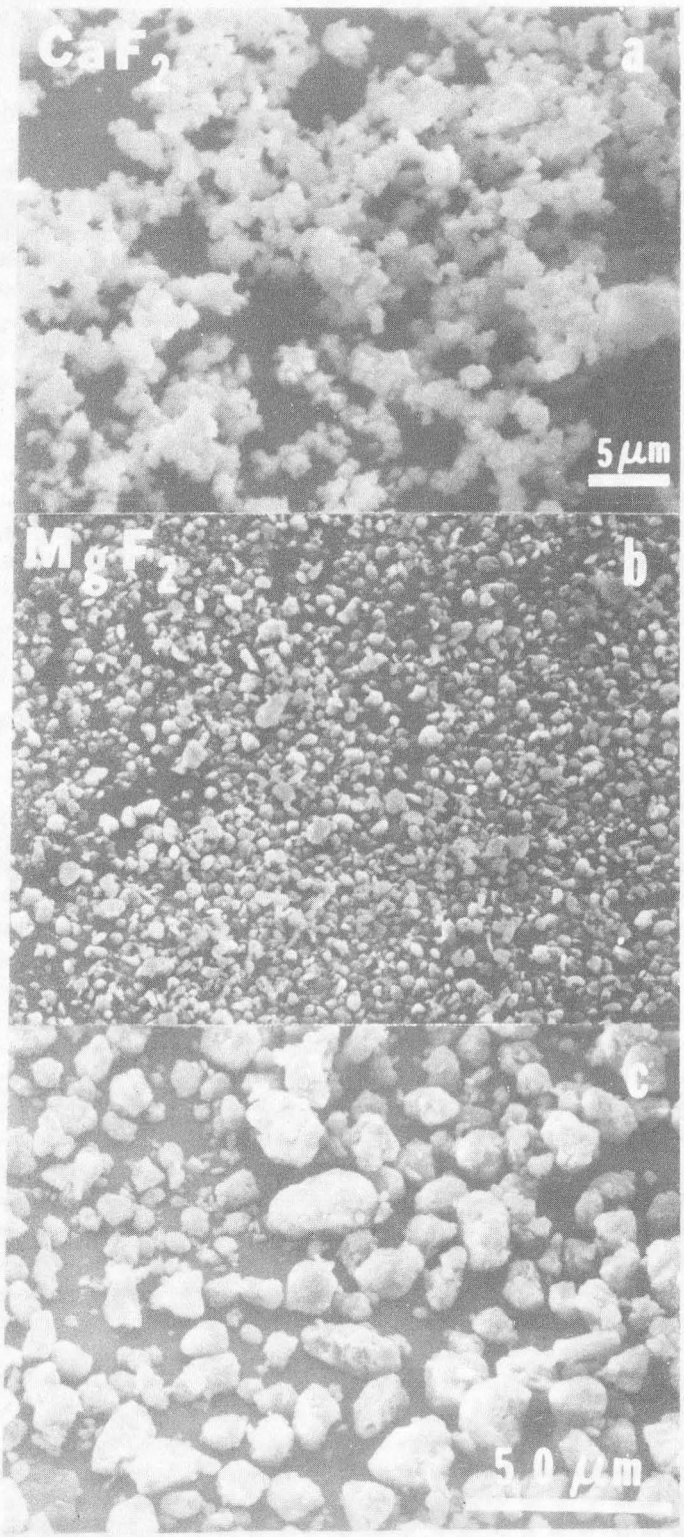

XBB 815-4301

Fig. 4

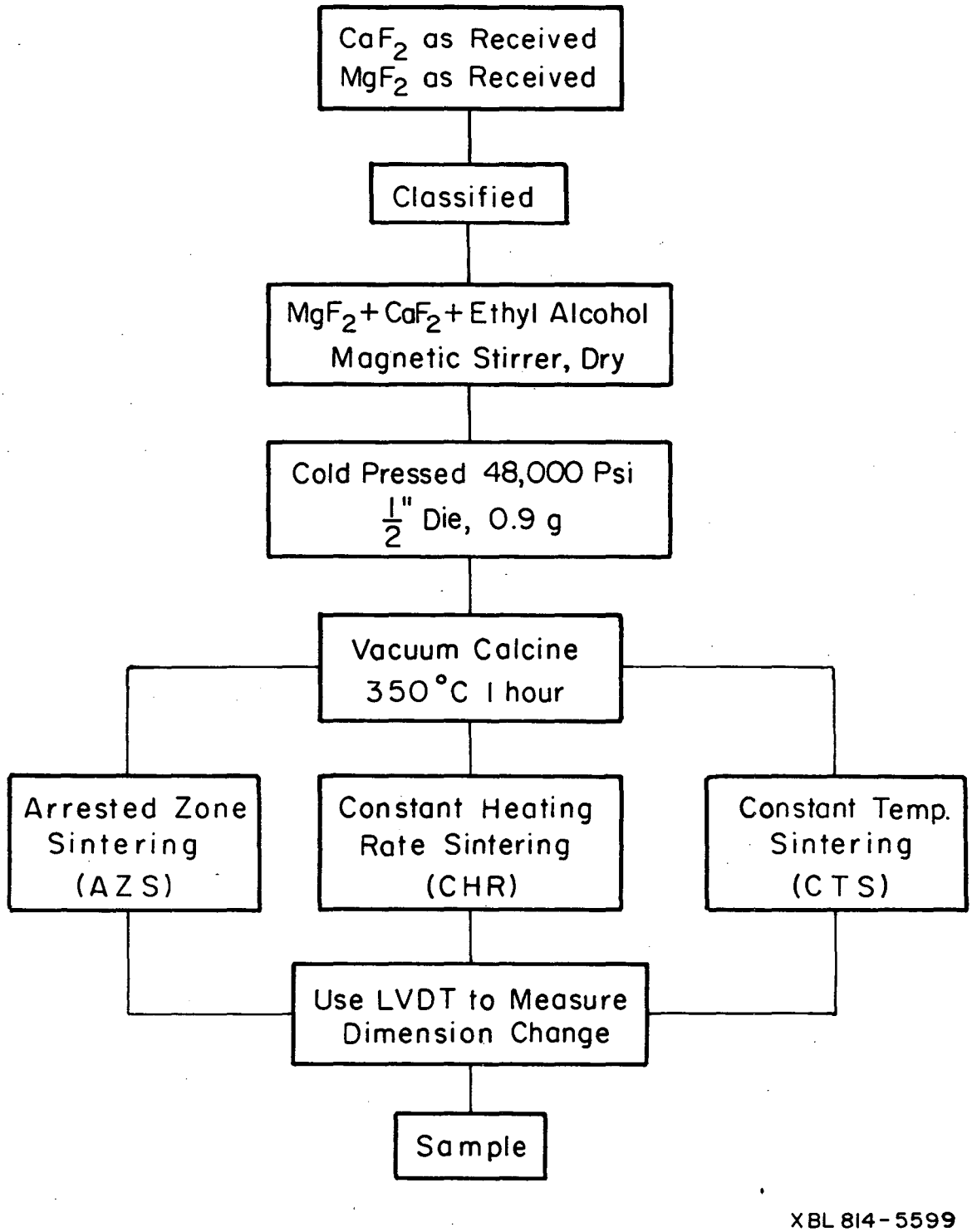
CaF_2 as Received
MgF_2 as Received
Classified
$MgF_2 + CaF_2$ + Ethyl Alcohol
Magnetic Stirrer, Dry
Cold Pressed 48,000 Psi
$\frac{1}{2}$" Die, 0.9 g
Vacuum Calcine
350 °C 1 hour
Arrested Zone Sintering (AZS)
Constant Heating Rate Sintering (CHR)
Constant Temp. Sintering (CTS)
Use LVDT to Measure Dimension Change
Sample
XBL 814-5599

Fig. 5

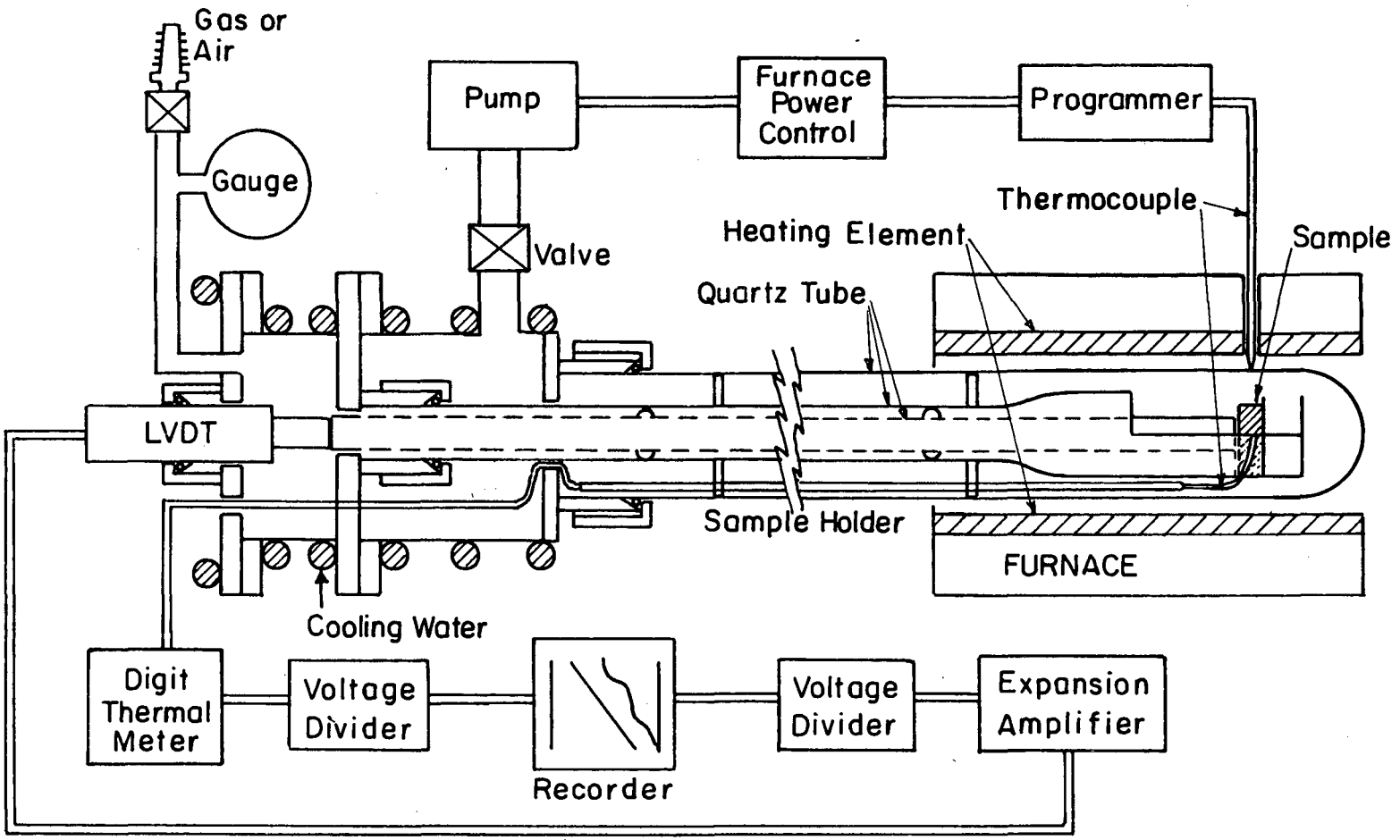

XBL 815-5663

Fig. 6

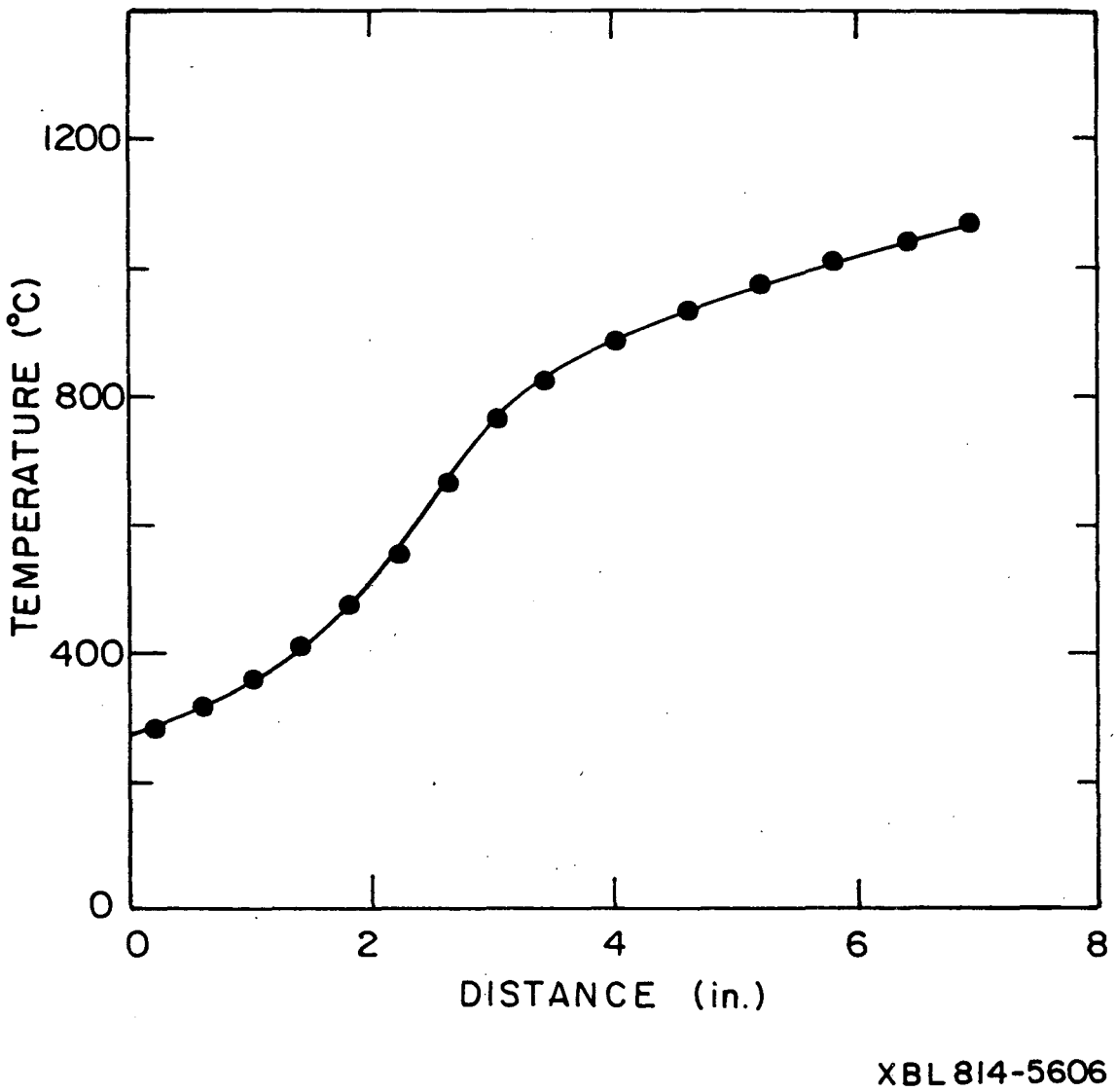

Fig. 7

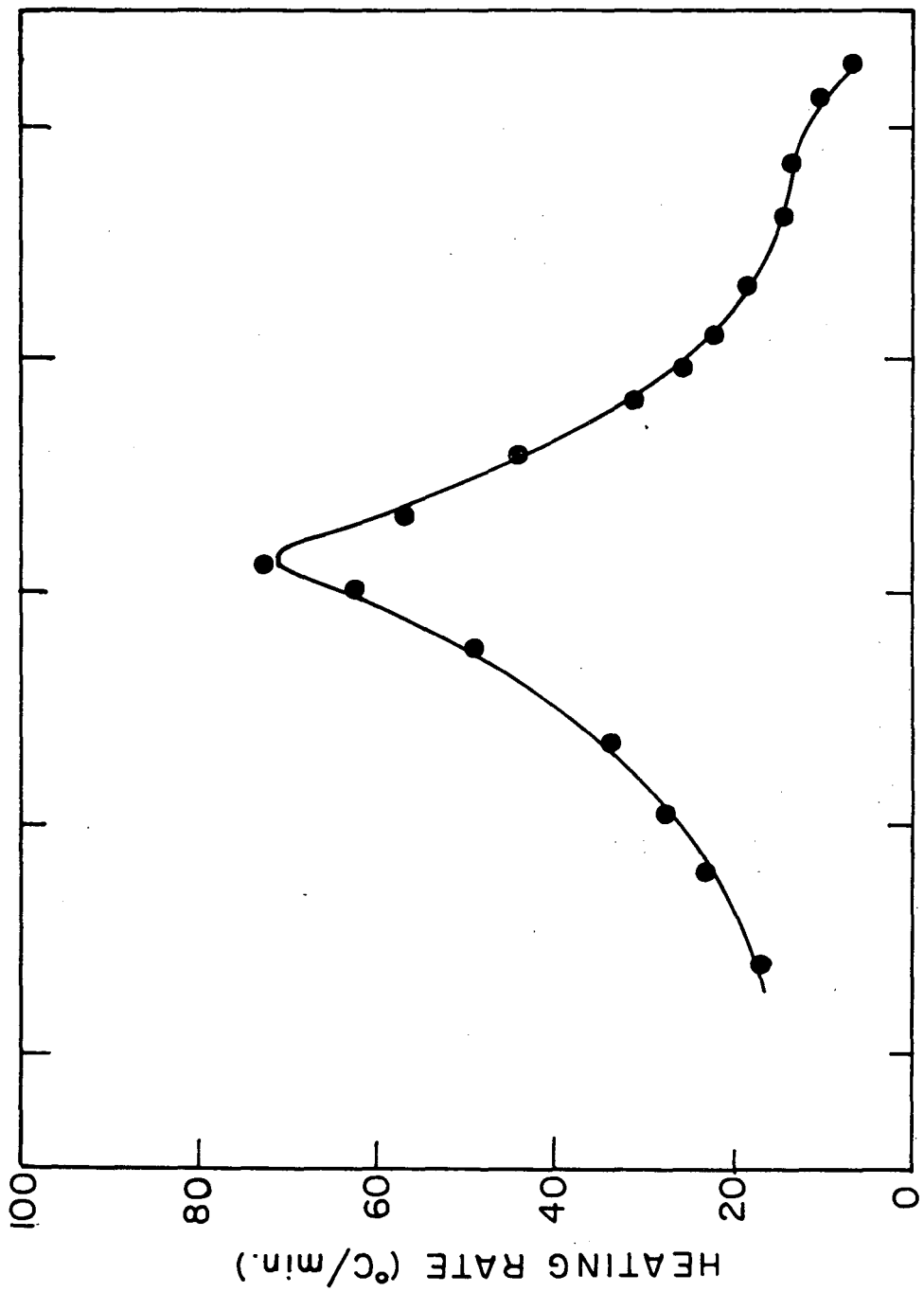
HEATING RATE (°C/min.)
0
20
40
60
80
100
200
400
600
800
1000
TEMPERATURE (°C)
XBL 814-5622

Fig. 8

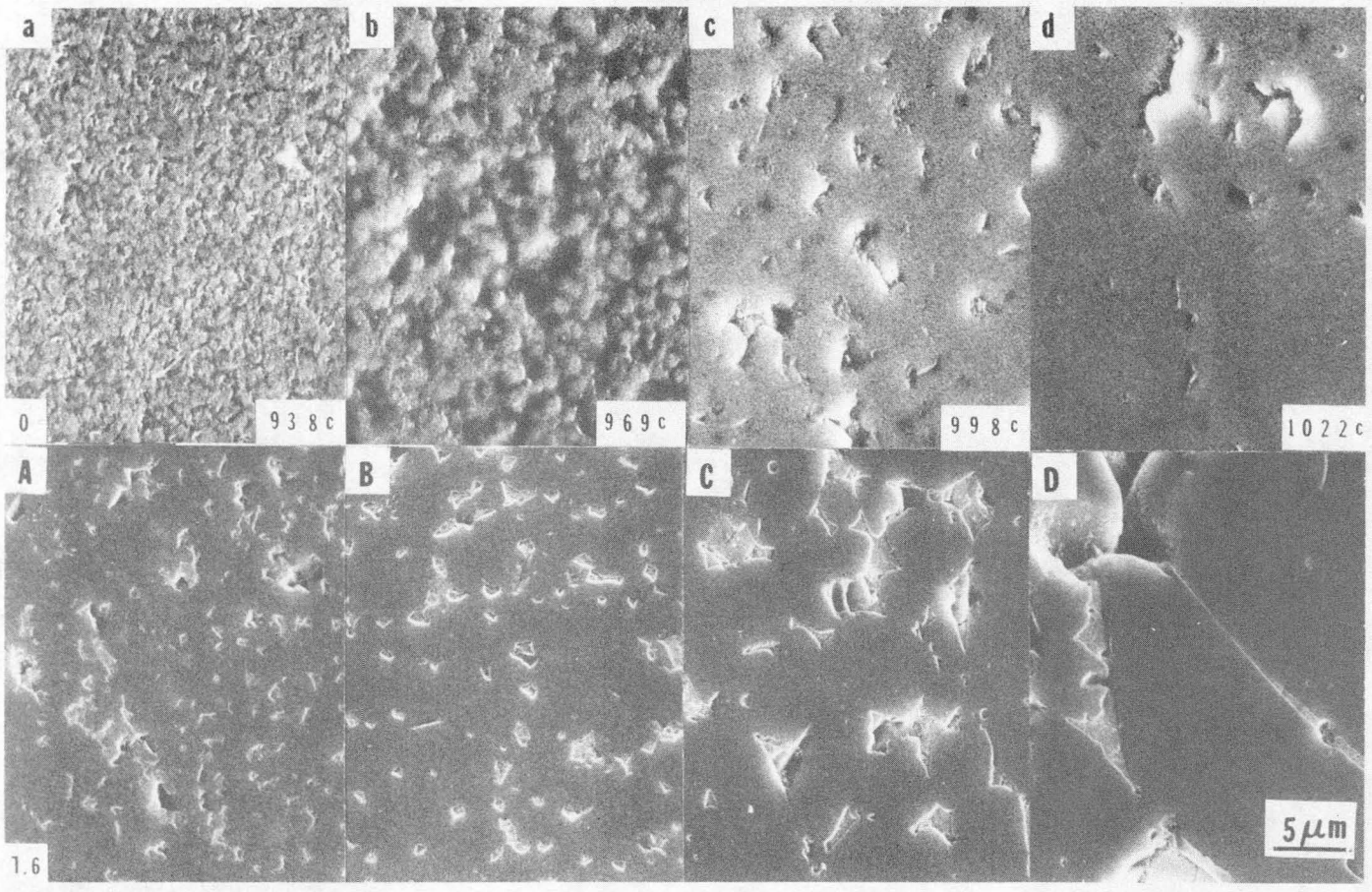

XBB 814-3807

Fig. 9

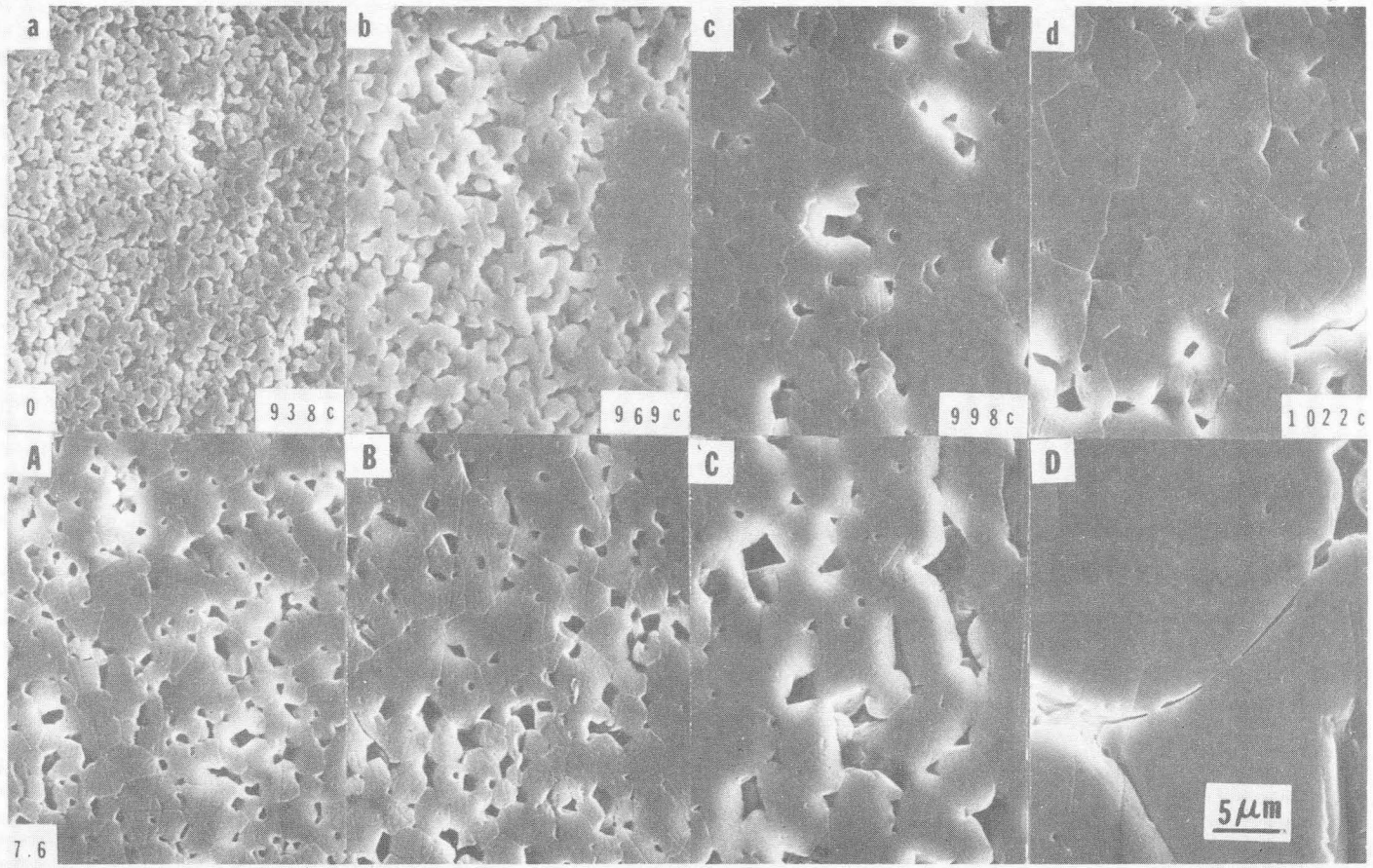

XBB 814-3808

Fig. 10

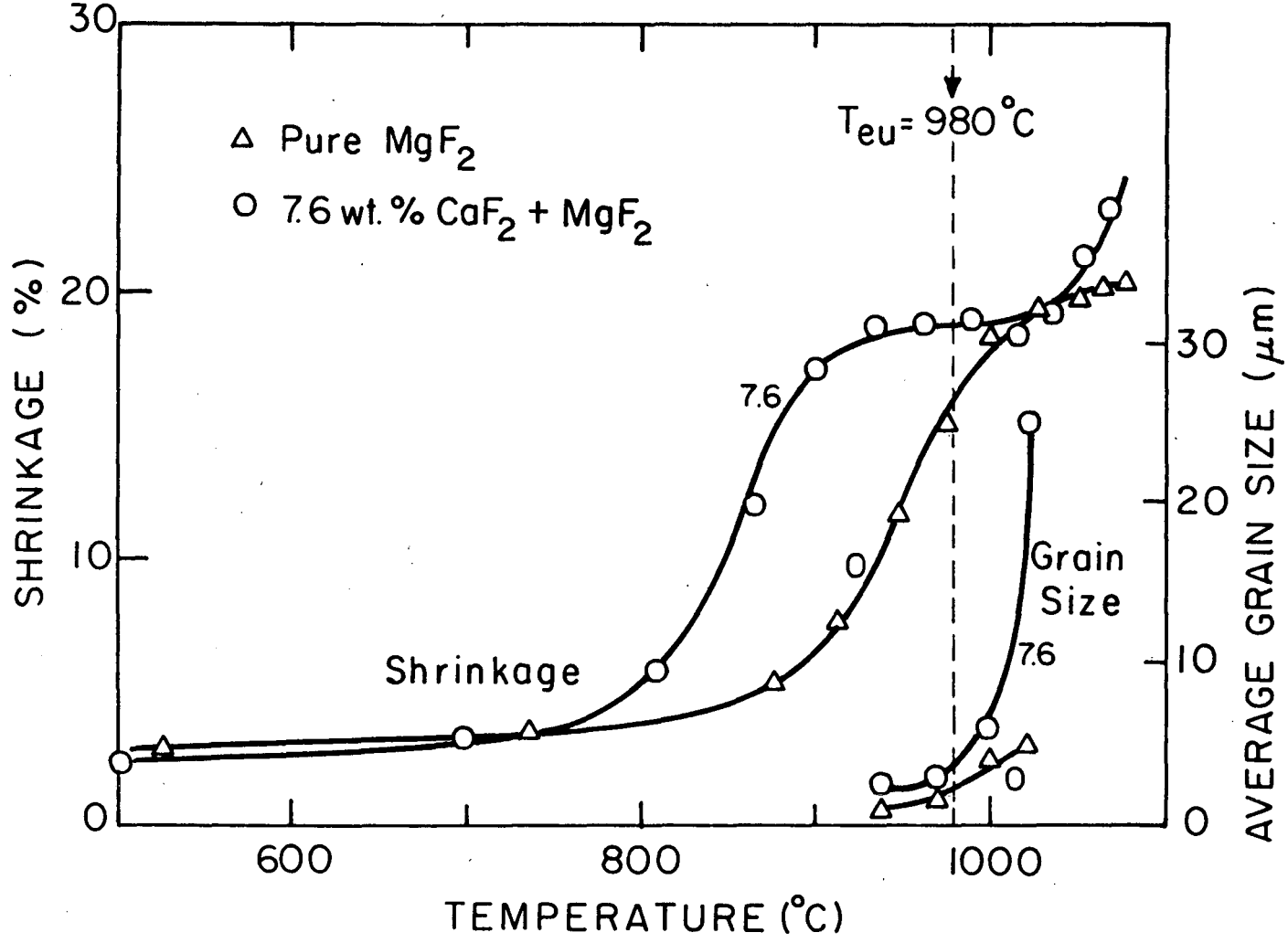

XBL 814-5601

Fig. 11

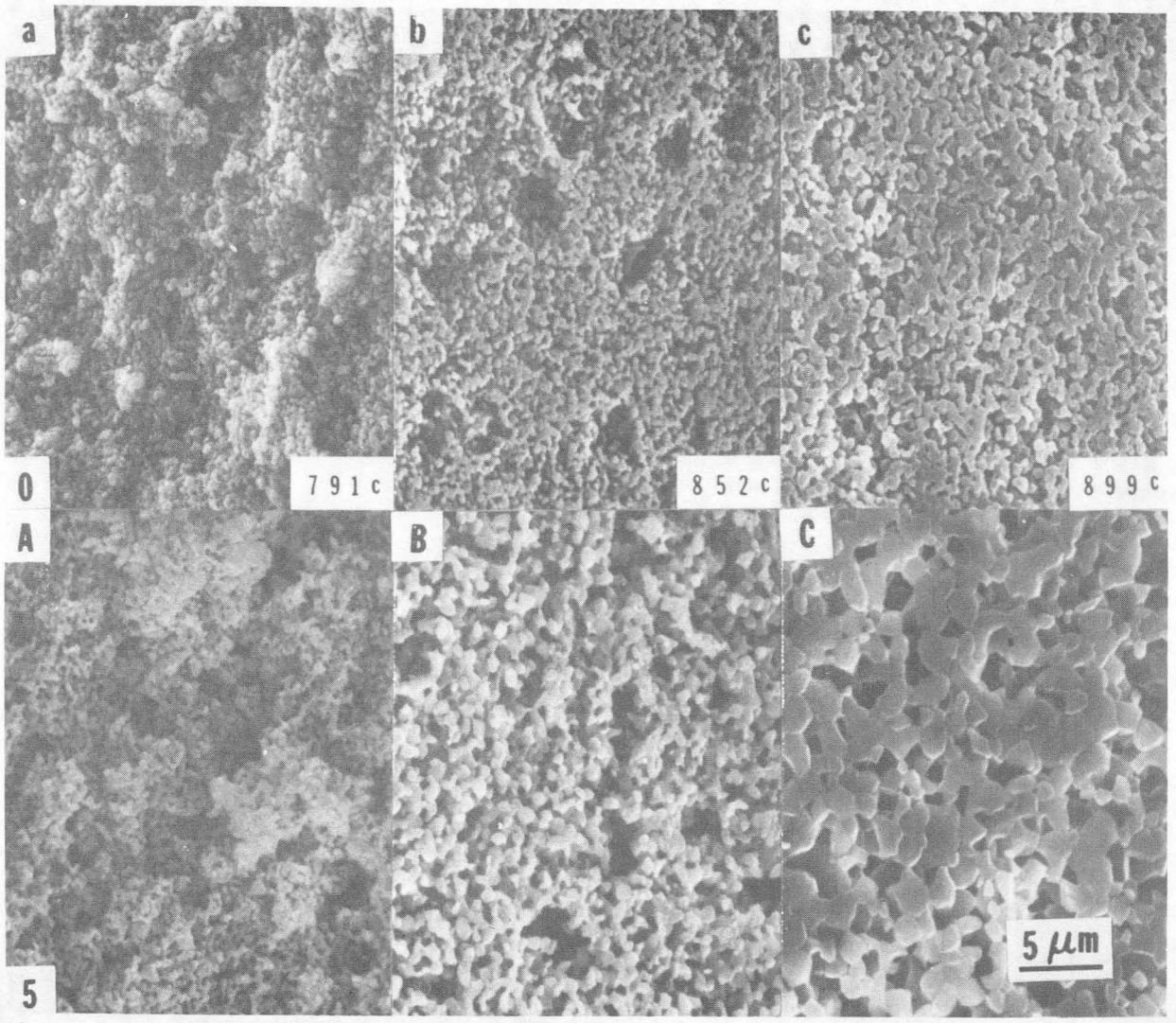

XBB 814-3806

Fig. 12

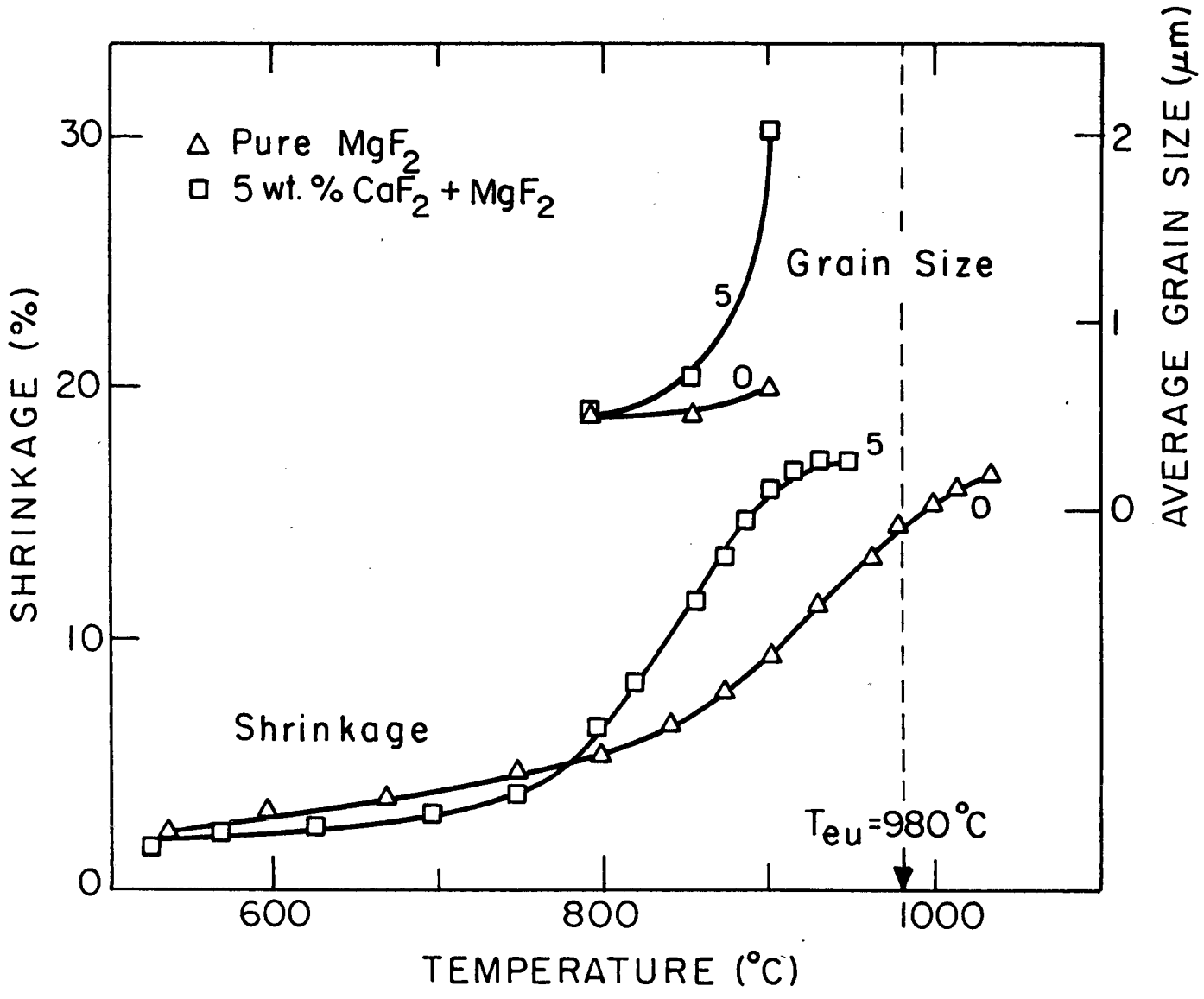

XBL 814-5600

Fig. 13

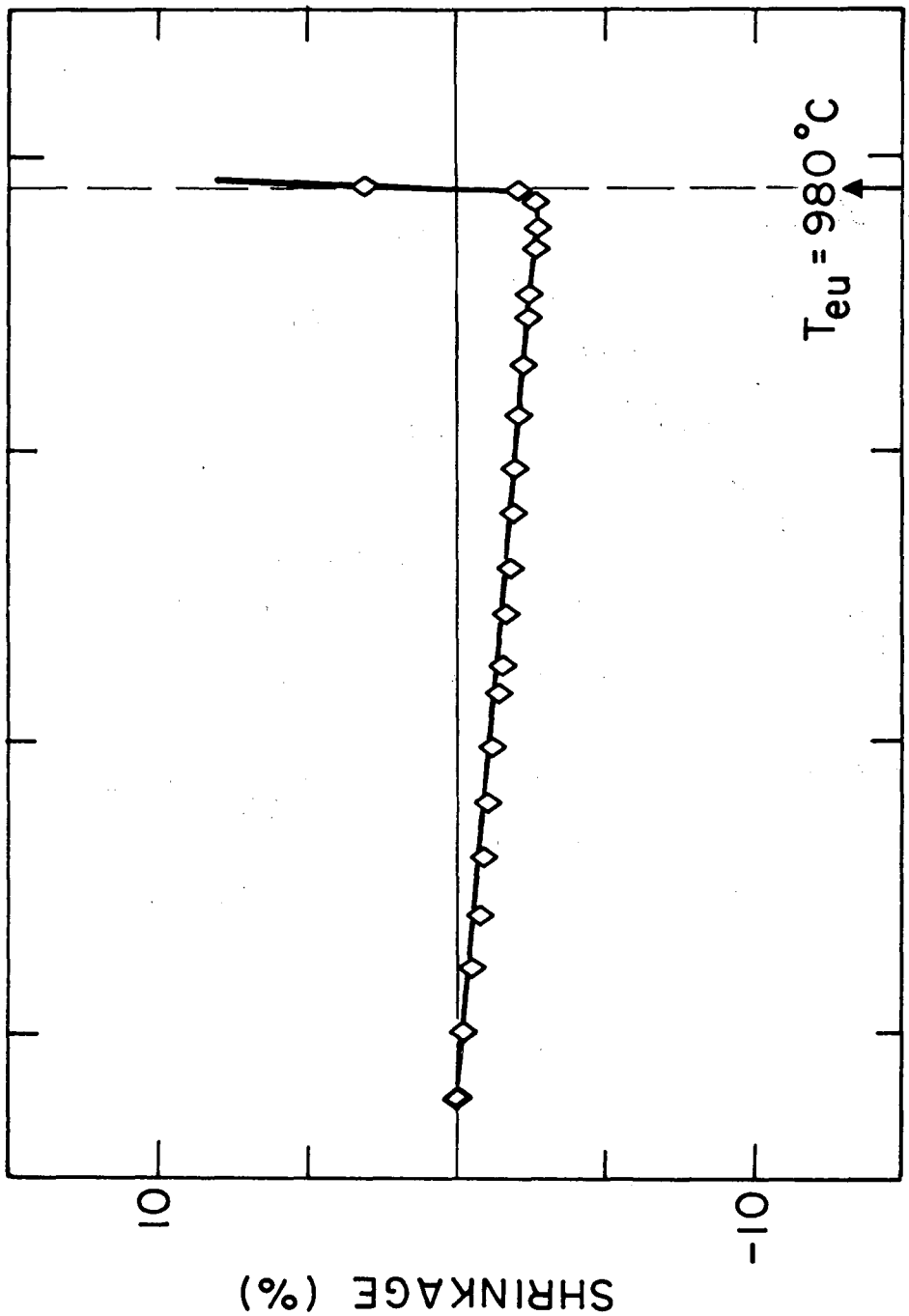

XBL 814-5602

Fig. 14

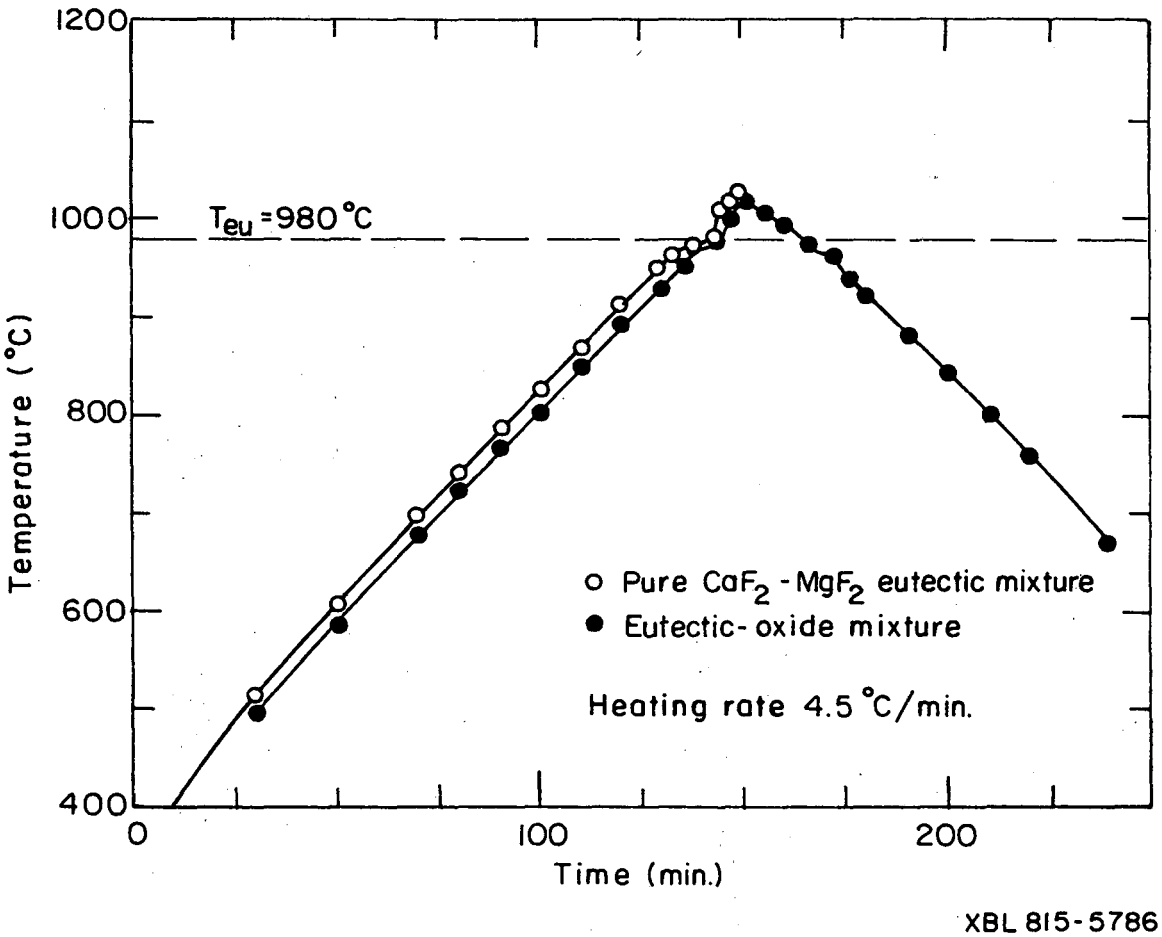
1200
1000
800
600
400
Temperature (°C)
T_{eu} = 980 °C
o Pure CaF_2 - MgF_2 eutectic mixture
● Eutectic-oxide mixture
Heating rate 4.5 °C/min.
0
100
200
Time (min.)
XBL 815-5786

Fig. 15

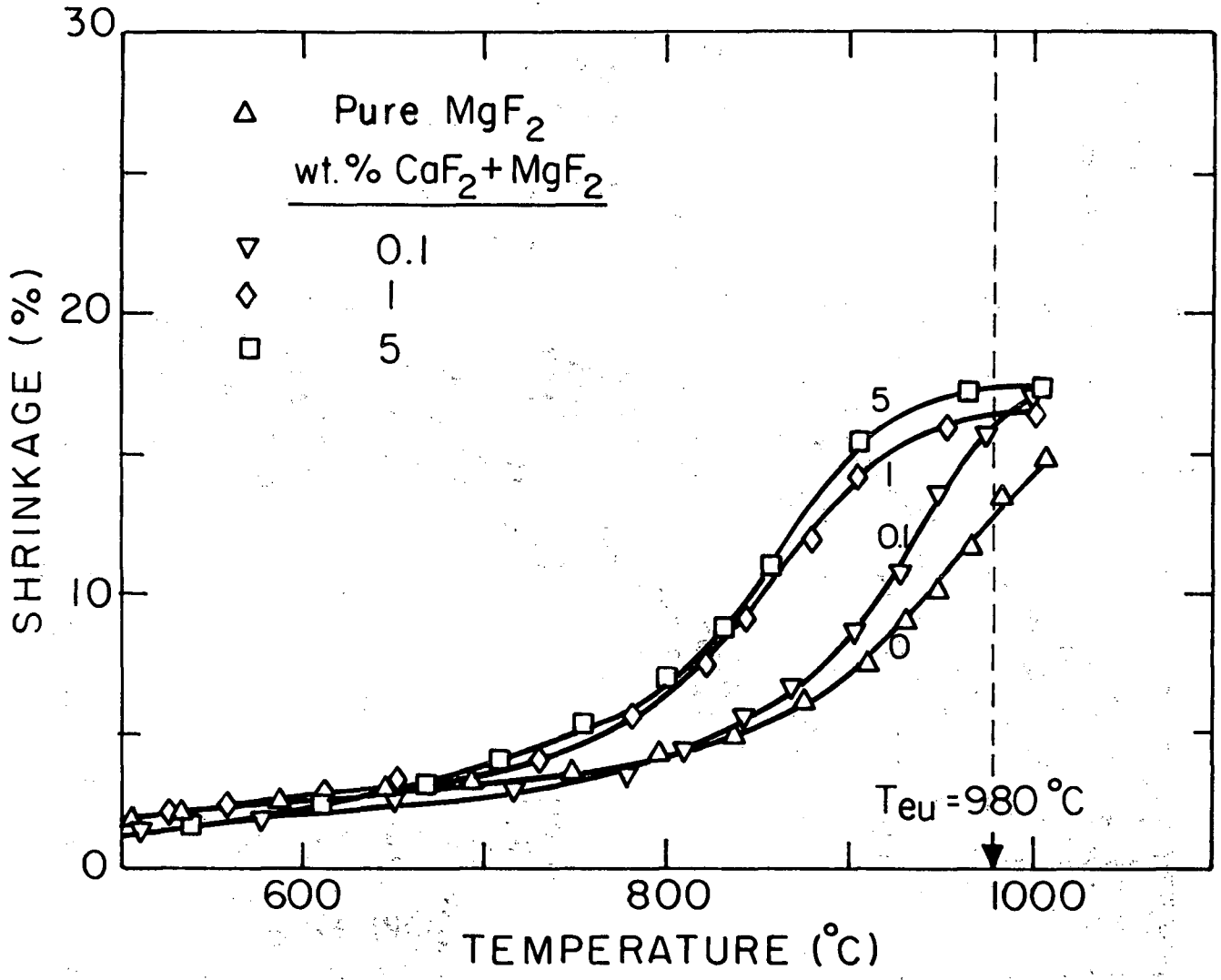

XBL 814-5597

Fig. 16A

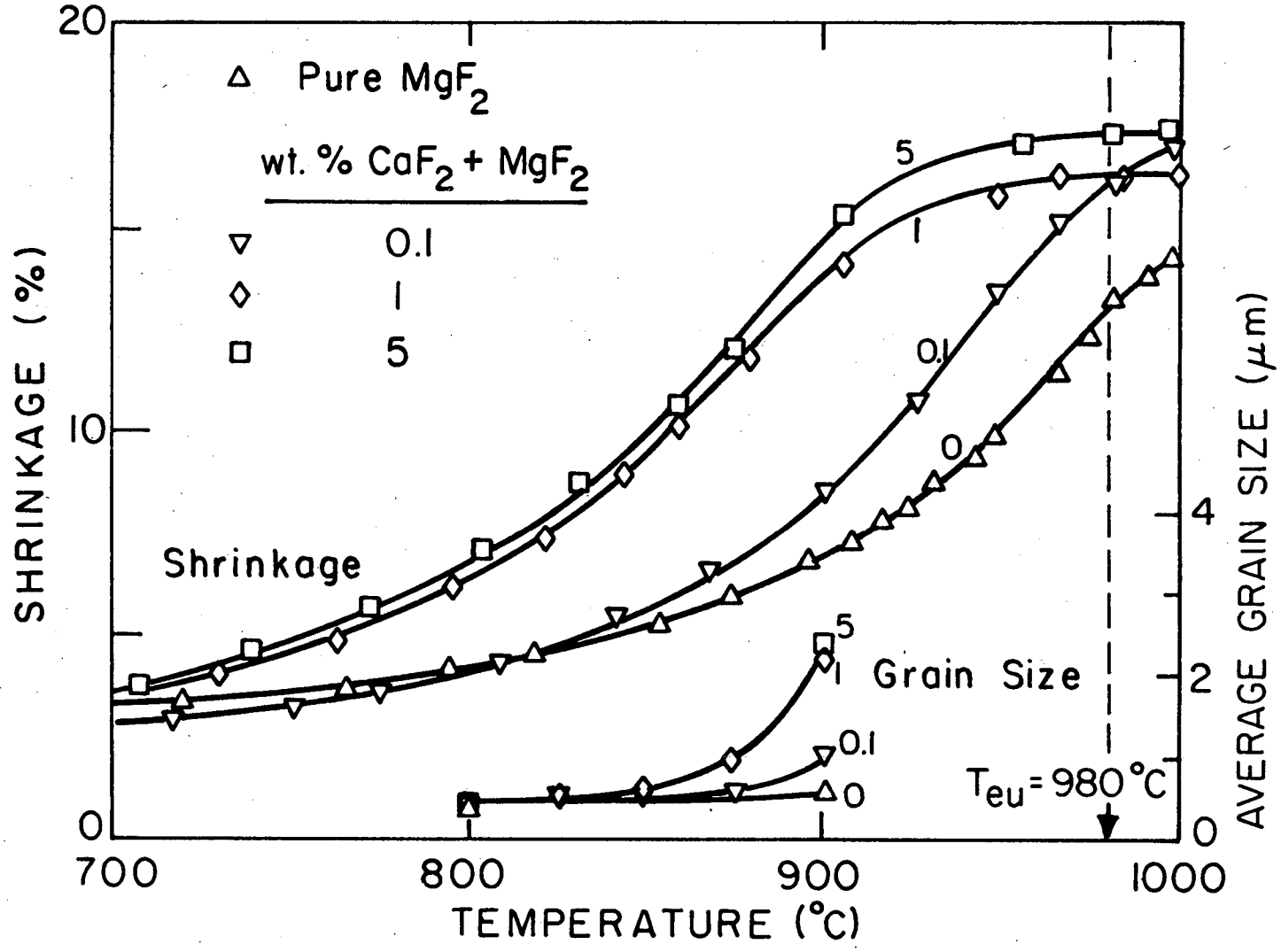

Fig. 16B

XBL 814-5598

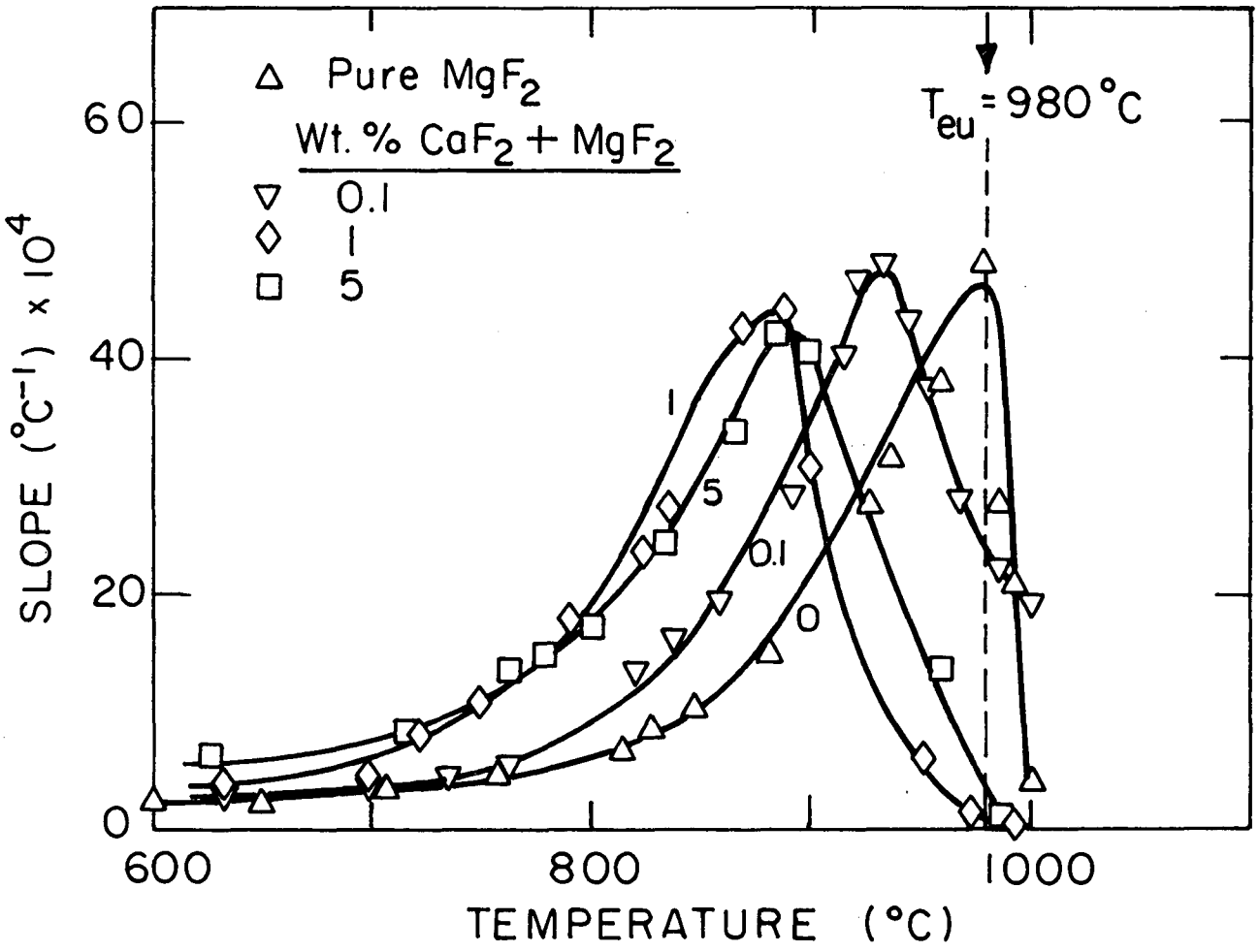

Fig. 17

XBL 814-5604

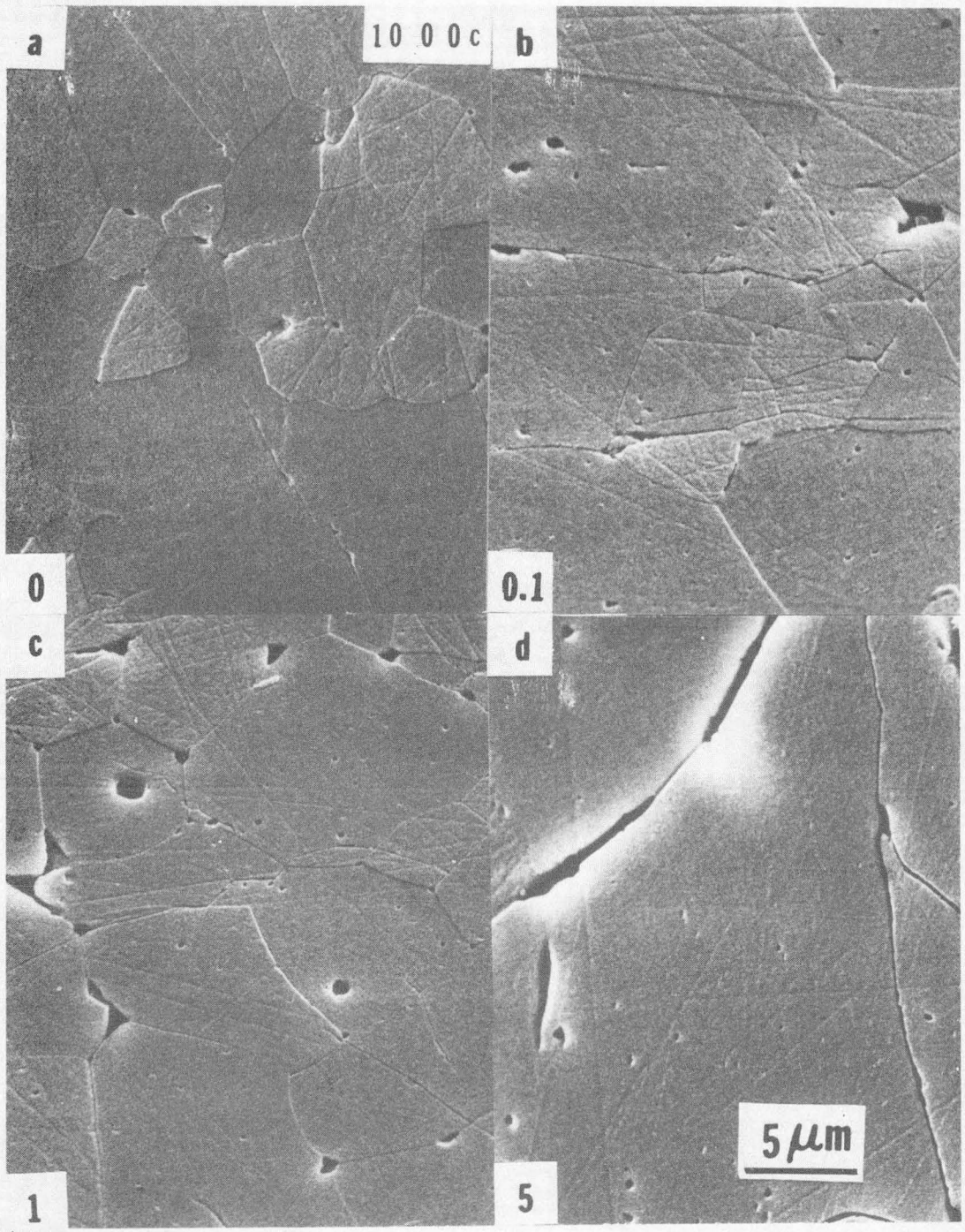

XBB 814-3804

Fig. 18

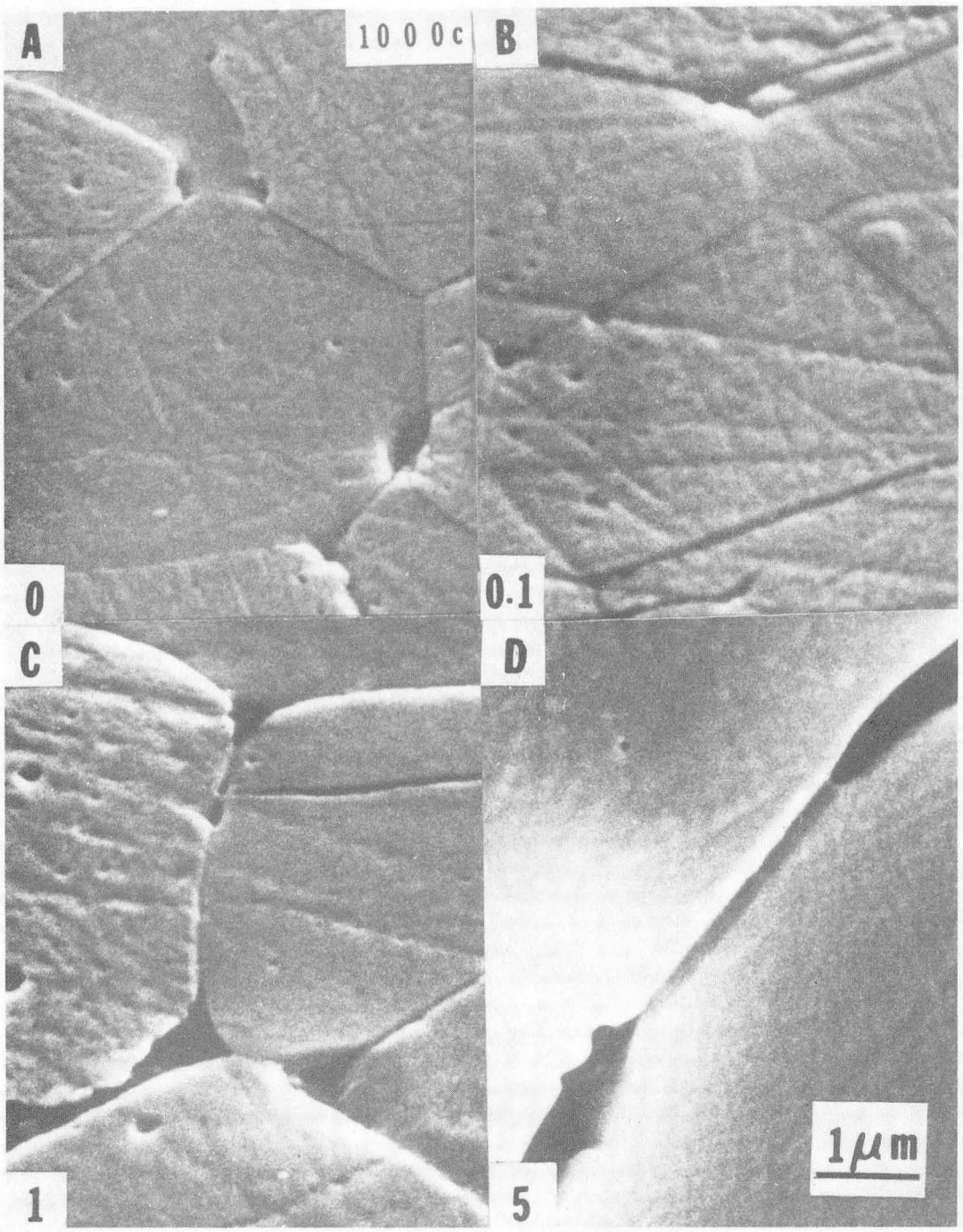

XBB 814-3800

Fig. 19

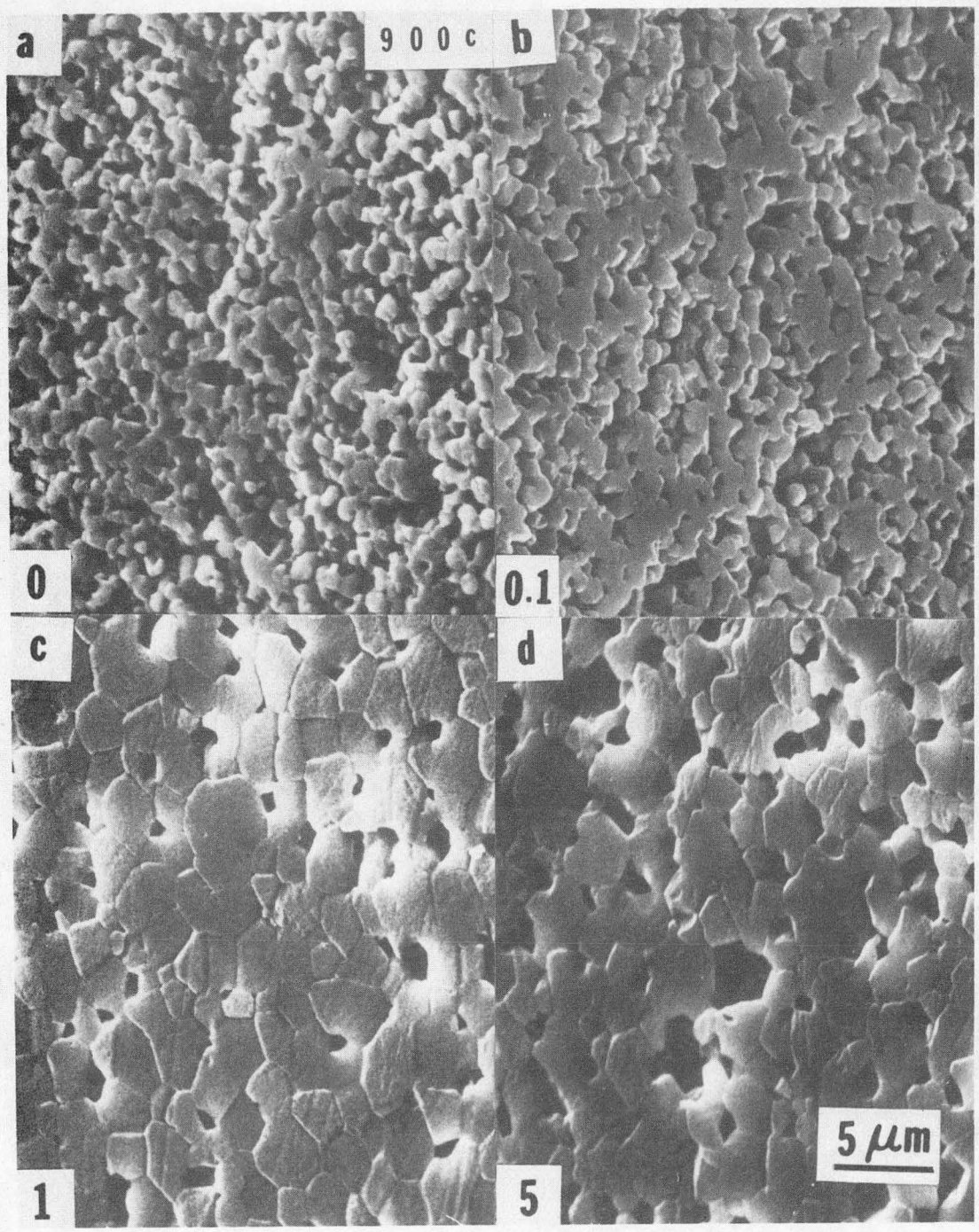

XBB 814-3802

Fig. 20

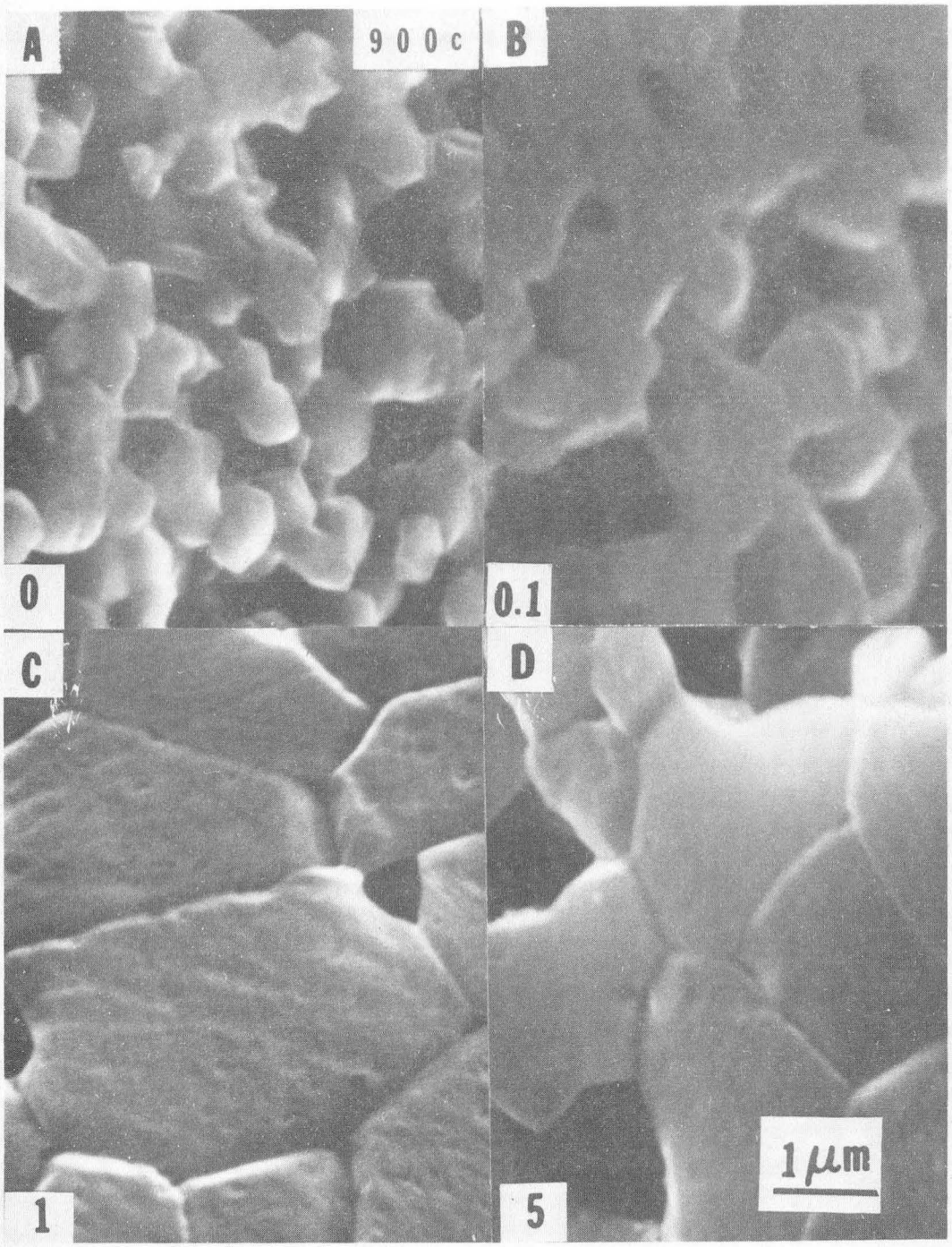

XBB 814-3801

Fig. 21

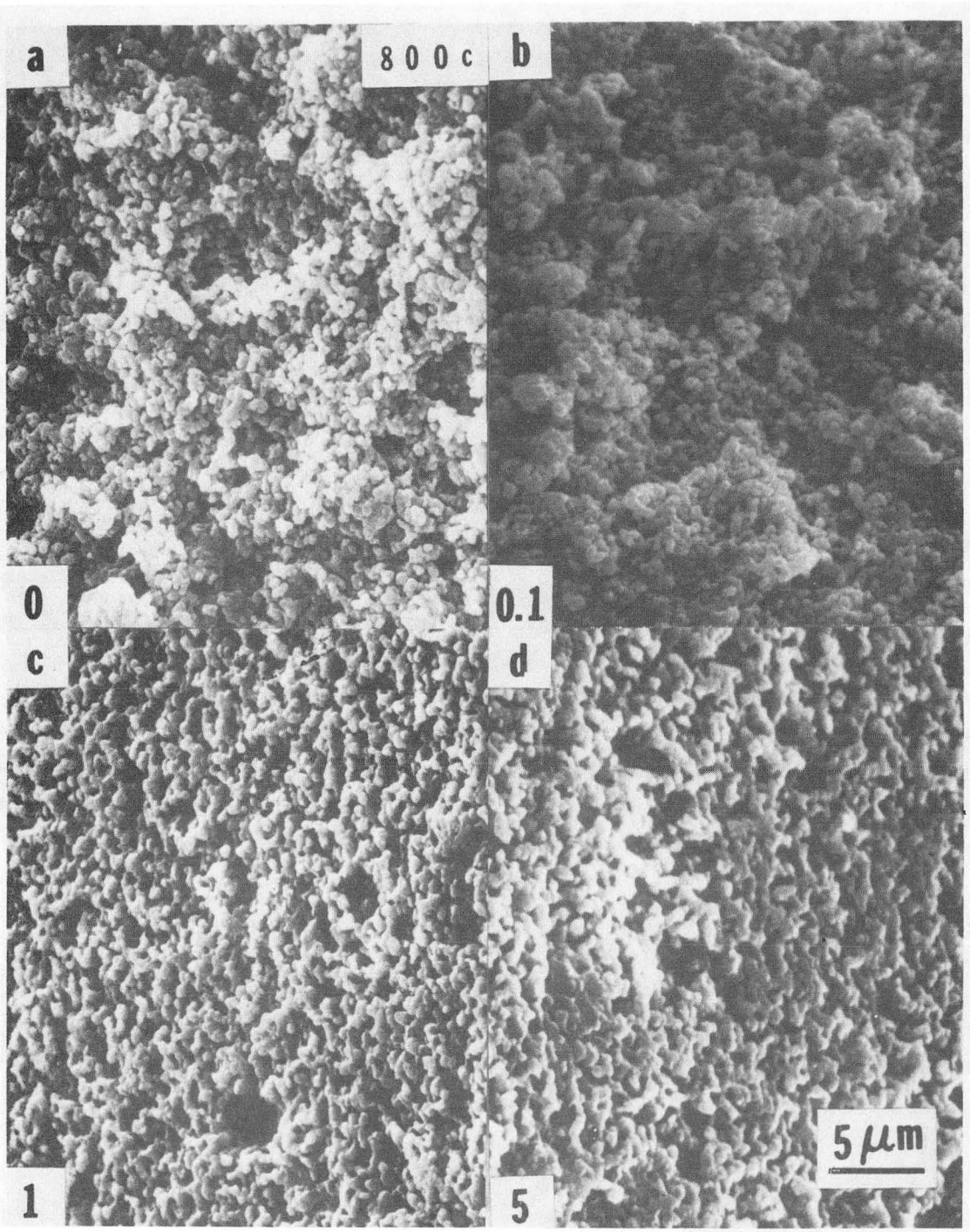

XBB 814-3803

Fig. 22

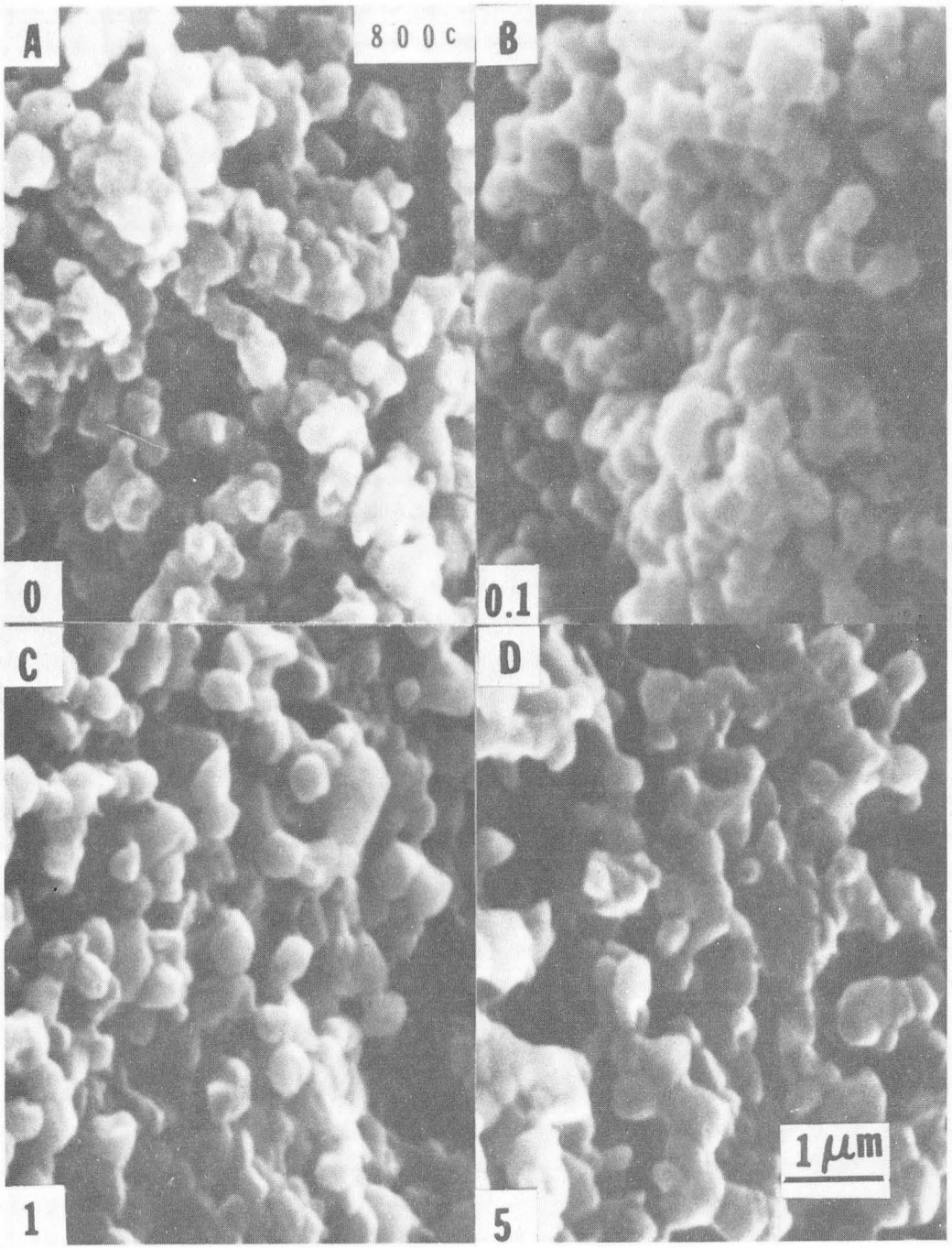

XBB 814-3805

Fig. 23

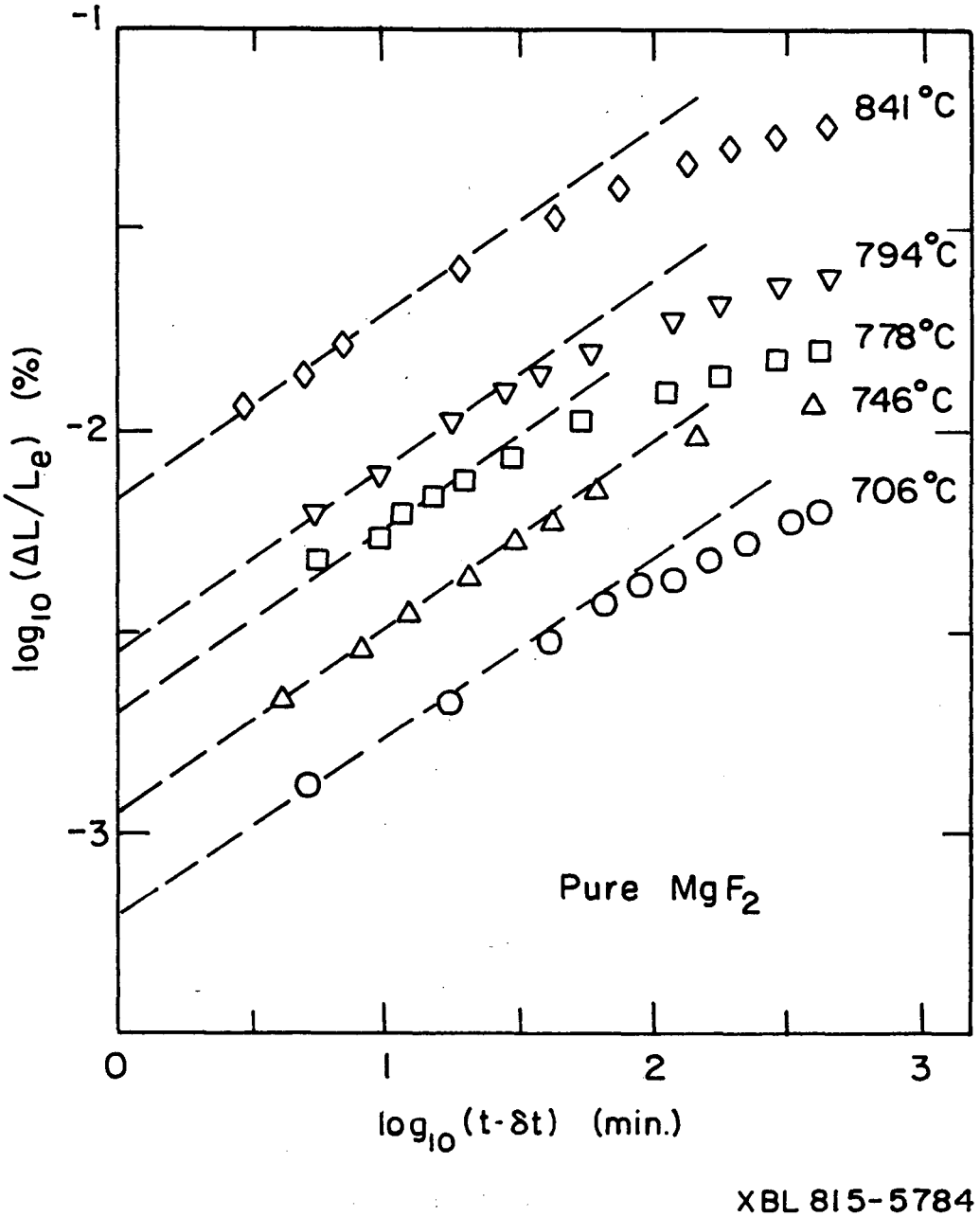
-1
-2
-3
0
1
2
3
841°C
794°C
778°C
746°C
706°C
Pure MgF2
log10 (ΔL/Le) (%)
log10 (t-δt) (min.)
XBL 815-5784

Fig. 24

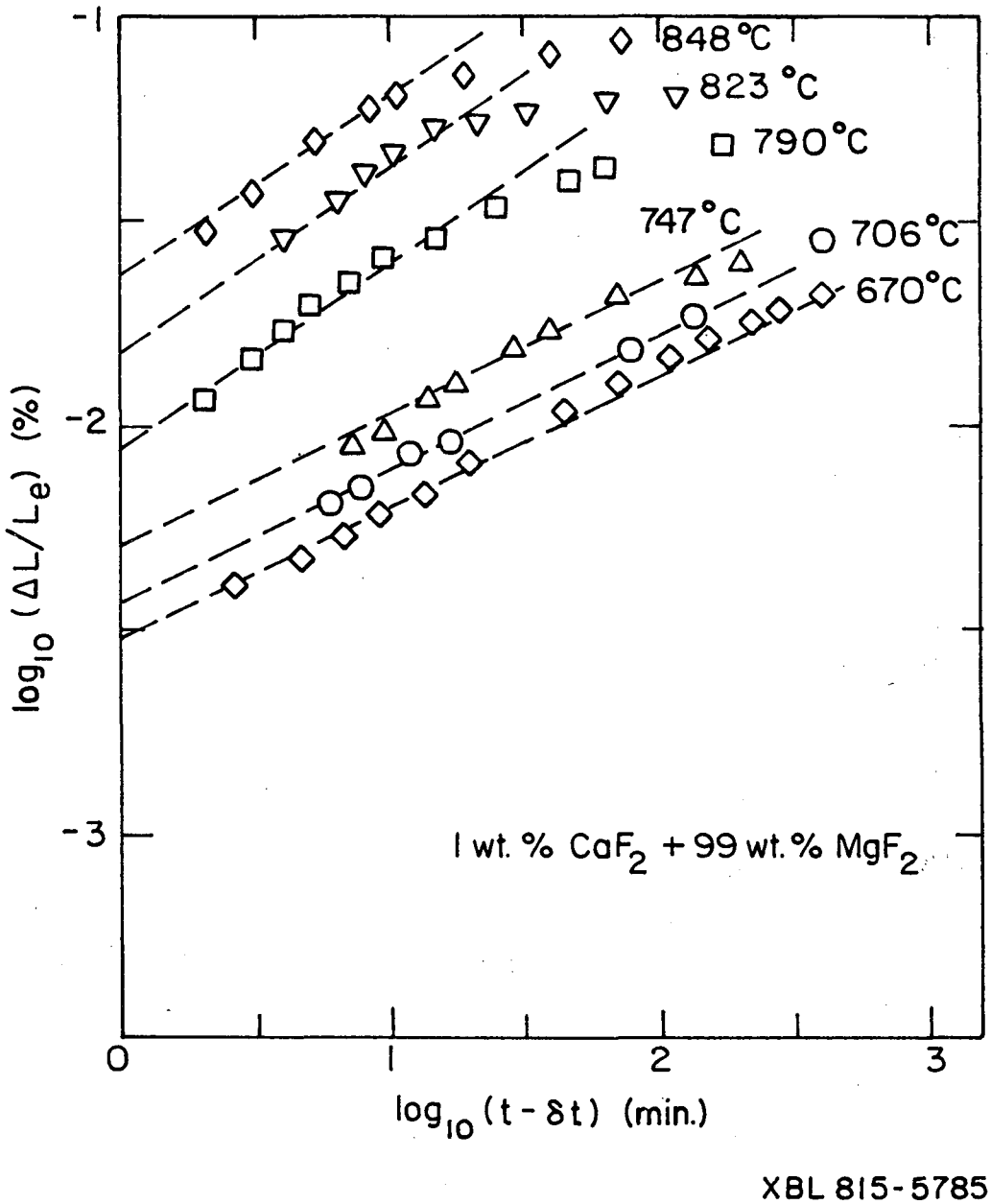
848°C
823°C
790°C
747°C
706°C
670°C
1 wt. % CaF2 + 99 wt. % MgF2
-1
-2
-3
0
1
2
3
log10 (ΔL/Le) (%)
log10 (t - δt) (min.)
XBL 815-5785

Fig. 25

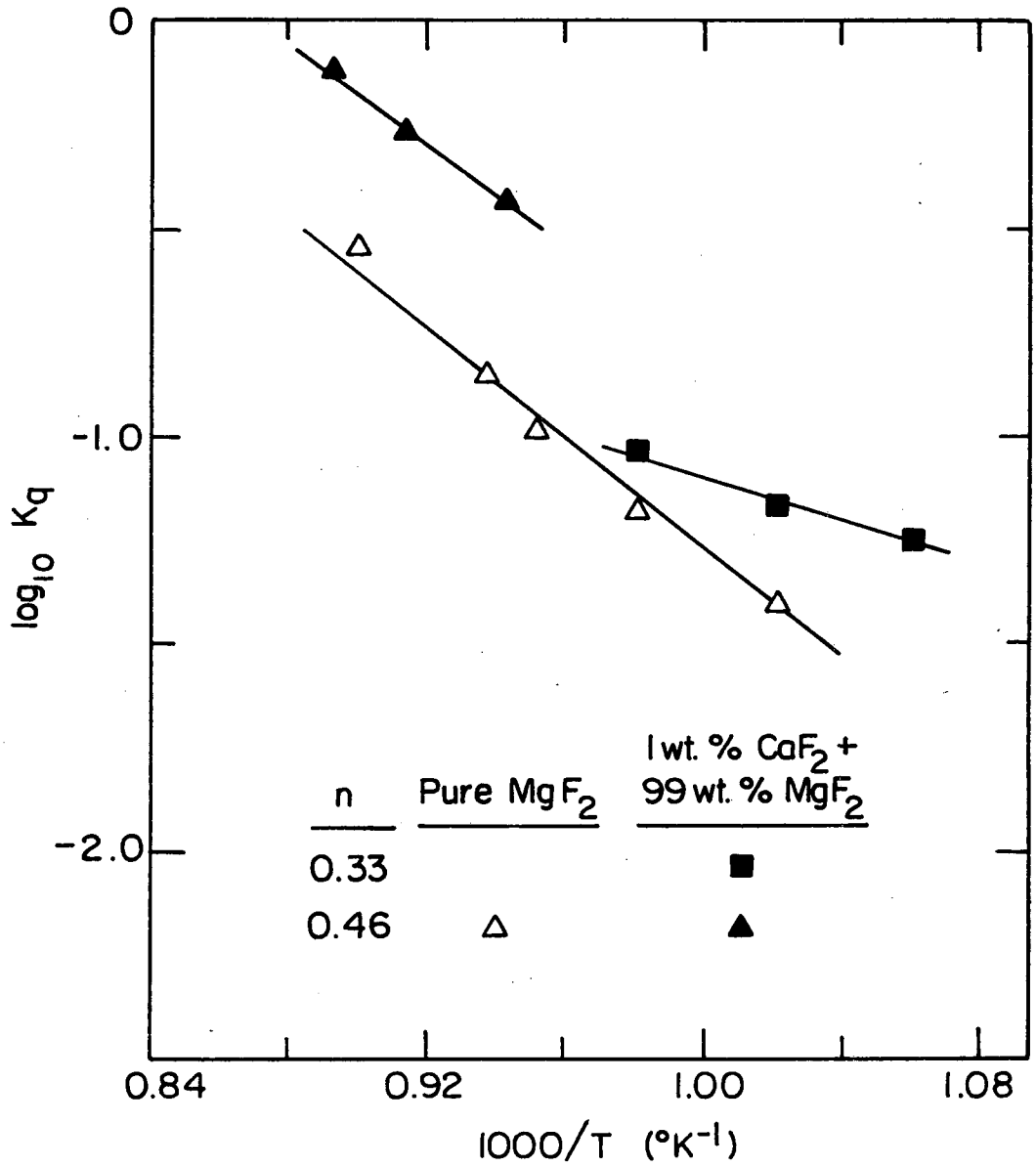
0
-1.0
-2.0
log10 Kq
n
Pure MgF2
1 wt. % CaF2 +
99 wt. % MgF2
0.33
0.46
0.84
0.92
1.00
1.08
1000/T (°K-1)
XBL 815-5783

Fig. 26

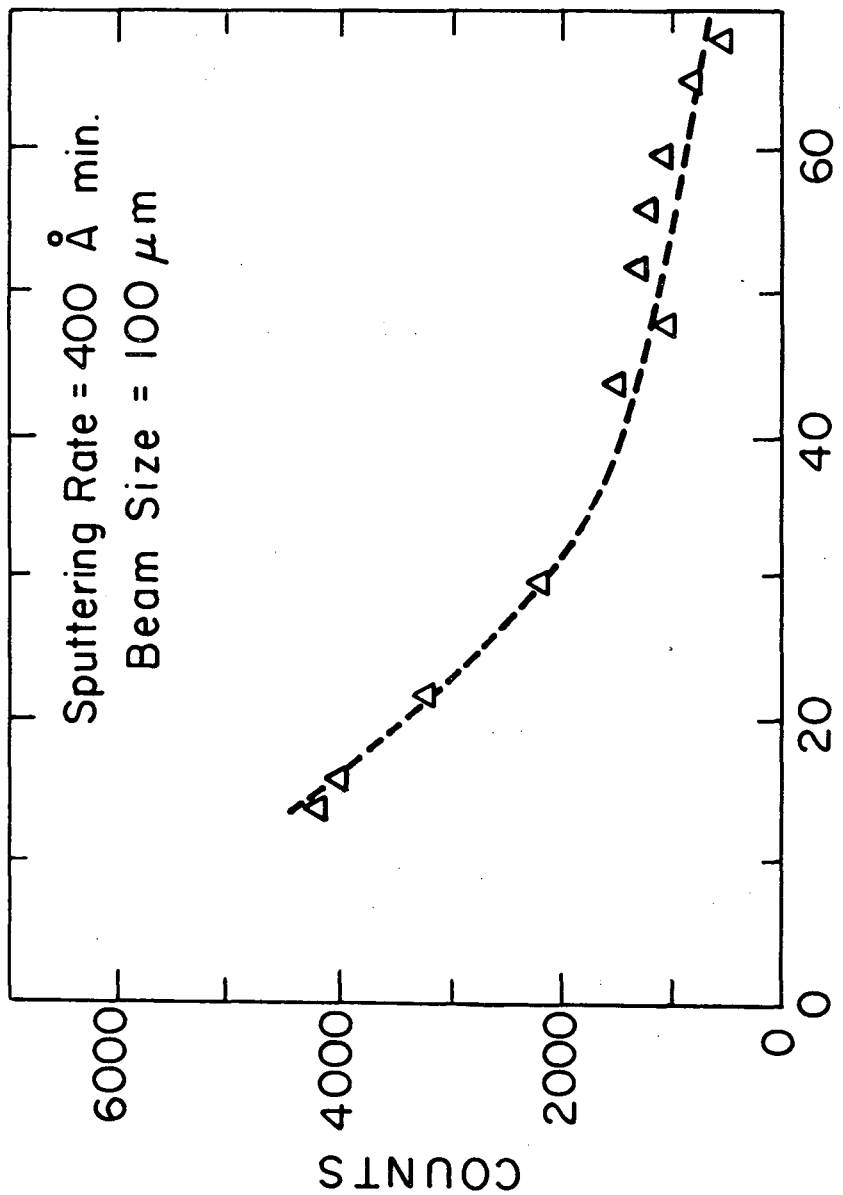

XBL814-5603

Fig. 27

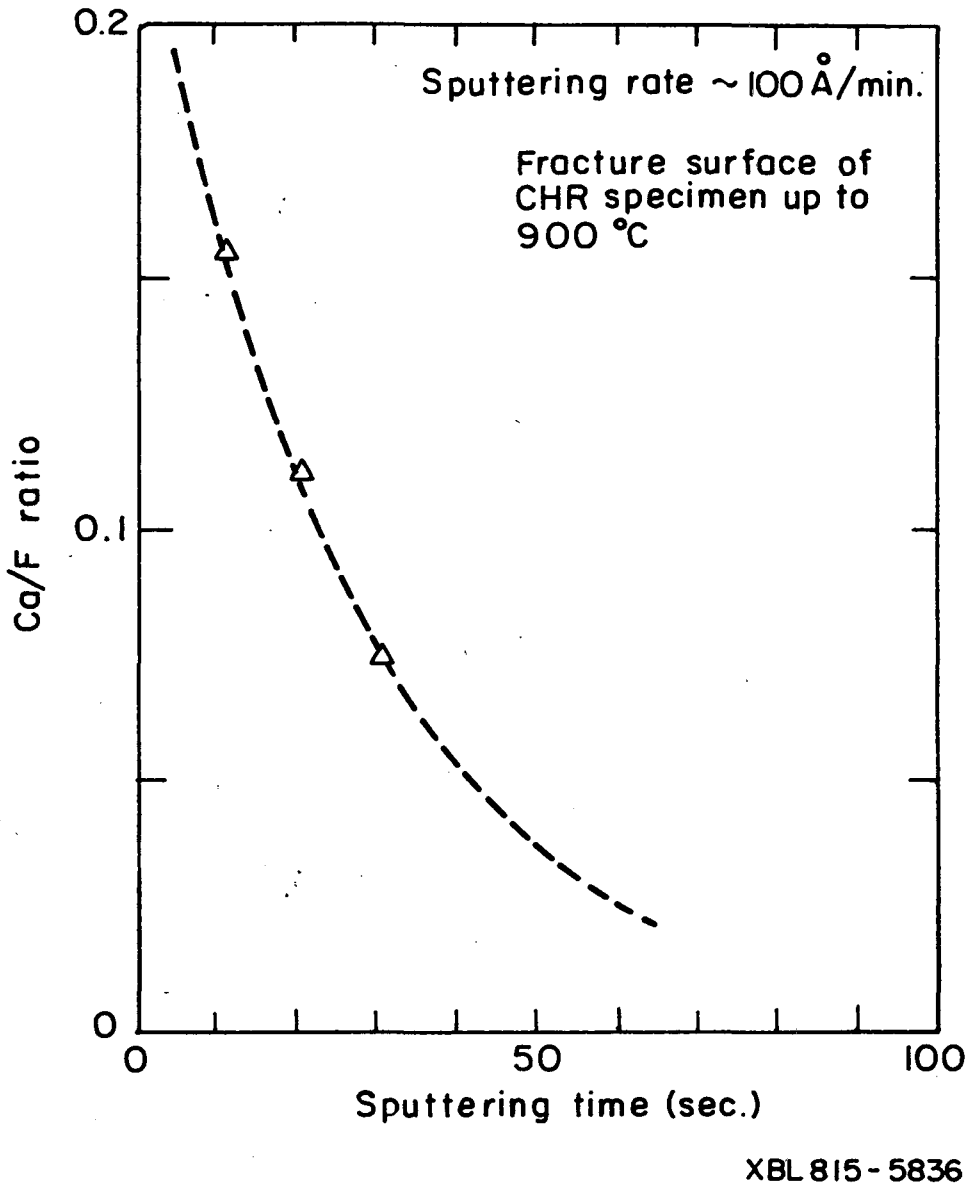
0.2
0.1
0
Ca/F ratio
Sputtering rate ~100 Å/min.
Fracture surface of
CHR specimen up to
900 °C
0
50
100
Sputtering time (sec.)
XBL 815-5836

Fig. 28

TECHNICAL INFORMATION DEPARTMENT
LAWRENCE BERKELEY LABORATORY
UNIVERSITY OF CALIFORNIA
BERKELEY, CALIFORNIA 94720